SOUTHWEST FISHERIES SCIENCE CENTER

NATIONAL MARINE FISHERIES SERVICE SOUTHWEST FISHERIES SCIENCE CENTER P.O. BOX 271 LA JOLLA, CA 92038

FEBRUARY 1999

MODELING PROPERTIES OF AIRBORNE LIDAR SURVEYS FOR EPIPELAGIC FISH

by

Nancy C.H. Lo, John R. Hunter, and James H. Churnside

ADMINISTRATIVE REPORT LJ-99-01

This Administrative Report is issued as an informal document to ensure prompt dissemination of preliminary results, interim reports and special studies. We recommend that it not be abstracted or cited.

MODELING PROPERTIES OF AIRBORNE LIDAR SURVEYS FOR EPIPELAGIC FISH

by

Nancy C. H. Lo,
John R. Hunter
National Marine Fisheries Service
Southwest Fisheries Science Center
P.O. Box 271
La Jolla, California 92038
Fax: 619-564-5656
Internet: nancy.lo@noaa.gov

and

James H. Churnside
Ocean Remote Sensing Division
Environmental Technology Laboratory
325 Broadway
Boulder, Colorado 80303

February 1999

TABLE OF CONTENTS

ABSTRACT

The objective of this study was to model various aspects of an airborne lidar survey system for small pelagic fishes (sardine, anchovy, and herring) with a focus on the features that might affect survey precision and accuracy. Modeling of the width of the swath cut by the laser indicated that swath width would have little or no effect on the rate schools would be encountered. Modeling of the proportion of schools that could be detected in typical coastal waters of California (α=0.1) indicated that about half of the schools would be detected by the lidar during the day and about 64% to 84 % during the night, depending on school packing density. A greater proportion of schools were detected during the night because small pelagic fishes have a shallow vertical distribution, while in the day schools may extend down to 155 m; and schools below about 40 m depth were not detectable to the laser. While schools tend to be more diffuse during the night than during the day, even the very diffuse night schools of anchovy (0.5 fish m^{-1}) are detectable throughout the upper 20 m of the water column with a lidar. A greater proportion of sardine schools was detectable during the night compared to the anchovy in our example because we used a packing density of 4 fish m^{-1} for sardine. At this density, about 84% of all sardine schools would be detectable during the night. With a substantial increase in instrument and survey costs it would be possible to increase the equivalent laser-pulsed-power by a factor of 10 over that of the "off-the-shelf system" used in our model. Such a change would increase the maximum detection depth by about 10 m, but would have negligible effect on the probability of detection of schools during the day due to the skewed vertical distribution of fish schools. More effective approaches for improving the accuracy and precision of potential lidar surveys for fisheries are to improve school detection algorithms and to develop a lidar survey model based on line transect theory. The depth limitations of lidar become an issue of survey precision rather than accuracy if a line transect model is used. Use of the model requires the synthesis of acoustic and lidar school distributions to produce an accurate reconstruction of the average vertical distribution of schools for a particular season and region, however.

1. INTRODUCTION

Airborne lidar surveys are an attractive alternative to the methods presently used for fishery-independent surveys of epipelagic fishes (Hunter and Churnside, 1995). They would cost much less per-survey-mile than ship-based methods (acoustic-trawl, ichthyoplankton), and the survey would extend to greater depth in the water than present aerial methods. A lidar, (li[ght] d[etecting] and r[anging]), in its most basic form, produces short pulses of laser light, which pass through the water surface and reflect off fish and particles in the water; a receiver measures the returning reflected pulse; the strength of the returning pulse separates fish targets from the reflectance of small particles, and the elapsed time indicates the range (depth below the surface) of the target. Fishery application of lidar technology is still in its infancy. Fish schools have been detected using a variety of lidar systems (Churnside and Hunter, 1996), but schools have never been systematically studied using lidar, nor has existing lidar technology been adapted to fish-survey needs; formal fish surveys have never been conducted.

A lidar survey system for fishery independent monitoring of epipelagic fish stocks is being developed jointly by two laboratories of National Oceanic Atmospheric Administration (NOAA) (Environmental Technical Laboratory, Boulder, CO; and Southwest Fisheries Science Center, La Jolla, CA). The approach is to combine evaluations of prototype instruments at sea with modeling of survey performance to develop an optimal lidar survey system. The goal is to develop a system that will deliver the greatest statistical precision for the lowest survey cost, while minimizing potential biases. In this paper, we model a lidar survey with the objective of evaluating possible trade-offs in instrument design affecting survey precision or accuracy. Two classes of trade-offs are considered, those affecting fish schools in the horizontal plane (swath width), and those affecting the detection of fish schools in the vertical plane (depth specific detection). We also analyze a trade-off between swath width and penetration depth which is analogous to changing from a visual-based aerial survey (wide swath, shallow penetration) to a lidar-based aerial survey (narrow swath, deeper penetration). We discuss each:

1.01 Swath width: Precision of an airborne lidar survey will depend upon the number of transects flown and probability of encountering schools along them. The width of the transect lines (swath width), may affect the probability of encountering schools and therefore could be one of the few factors affecting precision that involve instrument design. Swath width could be increased in a variety of ways (flying higher, scanning or optically expanding the laser beam) but such changes are accompanied by disadvantages (loss in penetration depth, reduced resolution, increased instrument cost and weight). In this paper we model how the width of the swath (width of transect line) cut by the survey instrument affects the probability of encountering fish schools, and therefore the precision of the survey estimate.

1.02 Depth specific detection: The accuracy of a biomass survey depends upon the extent the entire stock is vulnerable to the counting technique and the variability in the size of the uncounted fraction (Gunderson 1993). The key issue on accuracy for a lidar survey is the vulnerability of a stock to being counted in the vertical plane. Depth specific detection by a lidar depends upon:

laser power, sensitivity of the detection system, the rate of exponential decay of the laser pulse with water depth, the way the fish-detection function of the instrument changes with signal attenuation, fish size and reflectivity, school packing density and, of course, the vertical distribution of the fish. Using a set of models, we evaluated the effect of instrument and survey design on the accuracy of an aerial lidar survey for measuring fish abundance taking into account many of these variables. We consider how variations in laser power, school size, fish size, diel changes in vertical distribution of schools and school packing density would affect the accuracy of the survey. We also use these models to forecast the maximum depth that schools of anchovy, sardine and herring may be detected by a single lidar pulse.

2. METHODS

We used a variety of models to evaluate potential trade-offs in instrument and survey design. To evaluate how swath width may affect survey accuracy, two kinds of models were used: a simple encounter model and a school-group encounter model. To evaluate trade-offs between laser power and maximum detection depth for fish schools, we derive equations for the probability of detecting schools as a function of the signal-to-noise-ratio and develop equations for estimating laser power and the laser attenuation coefficient. School parameters, size, distribution and density, and survey area (46,204 km^2 =333 km (180 nm) x 138.75 km (75 nm)) were taken from acoustic surveys of northern anchovy in the Southern California Bight (Mais 1974; MacCall 1975[1]; Smith 1981; and Fiedler 1978). Vertical distributions of schools were based on northern anchovy off California (Holliday and Larsen 1979) for daytime and for night we used the distribution of early stage anchovy eggs (Pommeranz and Moser 1987), and acoustic data for anchoveta off Peru (Castillo V. 1995). Signal-to-noise ratio was based on the information of packing density of schools provided by Aoki and Inagaki 1988; Misund 1983; Graves 1977; and Freon et al. 1996.

2.01 The simple encounter swath model: The probability of encountering fish schools, p, is the probability that one transect line or swath will intercept one or more schools. If the swaths in a survey are perpendicular to the coastline, p can be computed from the following equation,

$$p_y = 1 - \prod_{i=1}^{n} [1 - \frac{(x_i + y)}{L}] \qquad \textbf{(1)}$$

where y is the swath width (meter), x_i is the diameter (meter) of the i^{th} school, n is the number of

[1]MacCall, A. 1975. Anchovy population survey simulation: A report of CalCOFI Anchovy Workshop Group on methods of estimating anchovy abundance, July 21-22, 1975, Contribution No. 4, 9 p.

fish schools and L is the length of the coastline. In the model, L=333 km (180 nm) which is about the length of the coastline in the Southern California Bight; the transect lines extended 138.75 km (75 nm) offshore bringing the total area surveyed to 46,204 km^2. Equation (1), the random encounter model, requires that schools be randomly distributed and is similar to the line intercept method (Eberhardt 1978).

Using Equation (1), we computed the encounter probability of schools (p_y), for schools of 30 m and 150 m diameter having abundance levels of 10 to 5000 schools in the survey area and the swath widths considered were <1, 10, 50, 100, 200, 500, 900 and 1600 m.

2.02 School Group Encounter Swath-Model: Many pelagic fish schools are not randomly distributed over the sea surface as required by Equation (1), but rather they are arranged in distinct aggregations or school groups (Cram and Hampton 1976; Fiedler 1978). The area of a fish school (expressed by school diameter in this paper) is highly variable as are the size and number of schools within a school group. Because of this complexity, simulations were used to compute the probability of encountering fish schools in a survey area (Fiedler 1978).

In the simulation, school groups are randomly assigned in the survey area. The sizes of the fish schools within a group were generated from the frequency distribution of the diameters of northern anchovy schools in the Southern California Bight (Fiedler 1978; Table 2 in Smith 1981, reproduced in Table 1). The number of fish schools within a fish school group was generated from the area occupied by the group and the density of schools. Both the diameters of school groups and the density of schools within a school group were assumed to follow lognormal distributions measured for anchovy in the Southern California Bight (Fiedler 1978; Smith 1981) (Figure 1). Simulations were used to compute the encounter probability (p_y) for various swath widths (y).

The locations of school groups were randomly allocated in north-south (n-s) and east-west (e-w) directions. When school groups overlapped (intersected) in the north-south directions, they were combined as a single group for computing the encounter probability. Only the north-south direction was relevant because the transect was run east-west. Schools were randomly allocated within a school group and overlapping schools in the north-south direction were combined as a 'single school' for computing purposes. This process continued until all schools were separated in the north-south direction and termed "disjoint schools." The distance (gaps) between disjoint schools in the north-south direction were summed for each school group and later they were summed for all fish groups. The sum of n-s gaps within school groups was termed as total_gap_within. Similarly, a total_gap_between (school groups) was also computed. Both total_gap_within and total_gap_between were used to compute the encounter probability.

The encounter probability for swath width y (p_y), similar to Equation(1), was computed for each iteration based on the gap length as

p_y = 1- (total_gap_within + total_gap_between)/L

or

$$p_y = 1 - \frac{\sum_{i}^{n}\sum_{j}^{J_i-1}(g_{ij}-y) + \sum_{i}^{n-1}(G_i-y) + E}{L}, \qquad (2)$$

where y is the swath width in meter, and g_{ij} is the gap length between jth and j+1th disjoint school within school group. The quantity of g_{ij} - y is set to zero if g_{ij} is less than y. G_i is the gap length between *i*th and *i+1*th disjoint school groups, and G_i - y is set to zero if G_i is less than y . E is the distance between the north and south end of the survey area and their nearest fish schools. n is number of school groups disjoint in the north-south direction and L=333 km (180 nm), the length of the coastline in the Southern California Bight.

Smith (1981) reported that the diameter (nm) of a school group followed a lognormal distribution with a logarithmic mean of 2.319 and a logarithmic variance of 0.676, and the density of fish schools/nm^2 in a school group had a logarithmic mean of 3.91 and a logarithmic variance of 0.51 based on data from MacCall 1975 [1]. The number of schools within a school group was the product of the area of the school group and the density of schools within. Thus, the mean number of schools in a school group was 10,274[2]. The diameter of fish schools was generated from the frequency distribution of the diameters of anchovy fish schools in the Southern California Bight (Table 1).

On average, there were 150,000 anchovy schools in the southern California Bight in the 1970s (Mais 1974). In recent years, the population has decreased to one fifth of that level (Jacobson et al. 1994). In the simulation, we constructed populations comprising 80,000, 32,000, and 16,000 schools with an average biomass of 12 mt . At each population level of anchovy, we simulated school groups for nine combinations of three school diameters and three school densities, each with a multiplier of 0.5, 1, and 1.5 applied to both mean and standard deviation of ln(school diameters) and ln(density of schools) respectively (Table 2). For example, for a population of 32,000 schools, a multiplier of 0.5 applied to both mean and standard deviation of ln(diameter) (an area of 9.45 nm^2 or 32.34 km^2) for a school group[3], and a multiplier of 1.5 applied to the mean and standard deviation of ln(density) (625 schools /nm^2 or 182 schools/km^2)[4], yield an average number of 5914 schools /school group, and an average of six school groups (32000/5914). This population will be denoted as 32000(0.5,1.5). The encounter probabilities for seven swath widths: 1, 10, 50, 200, 500, 900, and 1600 m for a total of 63 (3 x 3 x 7) sets of scenarios were simulated (in computation, numeral 1 was used t o represent diameters less than or equal to 1 m). For each of three populations, 500 iterations were run for each of 63 sets. The mean of encounter probabilities from 500 runs was used to estimate the mean encounter probability.

For multiple swaths (n), the probability($p_{y,n}$) that at least one of the swaths intercepts any schools is:

$$p_{y,n}=1-(1-p_y)^n \quad , \qquad \textbf{(3)}$$

---

[2]The mean diameter is 14.25 nm= exp(2.319+0.676/2) and the mean density of fish schools is 64.39 schools/nm2=exp(3.91+0.51/2), the mean number of fish schools in a school group =$(14.25/2)^2 \pi$ 64.39 =10,274

[3][exp(2.319*0.5+0.676*0.5*0.5/2)/2]^2 * 3.1416 =9.45

[4]exp(3.91* 1.5 +0.51*1.5*1.5/2) = 625.62

where p_y is computed from either Equation(1) or (2).

2.03 Estimating the number of swaths needed in a survey: Typically, the optimal sample size for a survey is computed by minimizing the variance of the estimate subject to a fixed cost. Since this information is not available, we define a desirable sample size in terms of the minimum number of transect lines or swaths needed to guarantee at least one positive sighting at an acceptable probability. Therefore, based on p_y from Equation(1) or (2), one can compute the number of swaths (n) needed for a desired value of $p_{y,n}$ using

$$n = \frac{\ln(1-p_{y,n})}{\ln(1-p_y)} \qquad (4)$$

2.04 Probability of detecting fish by depth using signal-to-noise ratios (SNR): The signal level of a lidar system decays exponentially with depth. The decaying signal of a single pulse can be expressed by

$$S(z) = S_0 \frac{\beta_w(z) + \beta_f(z)}{\beta_0} \exp(-2\alpha z), \qquad (5)$$

where z is depth in meters, S_0 is the signal level at the surface, β_w is the clear-water backscatter coefficient, β_f is the backscatter coefficient of a school of fish, β_0 is the backscatter coefficient at the surface, and α is the lidar attenuation coefficient. The backscatter coefficients, β, have units of m^{-1} and represent the fraction of the energy that would be scattered upward by a 1 m layer of either clear water or fish. By clear water we mean natural sea water with its attendant load of yellow substance, plankton, silt, etc., but without fish. The lidar attenuation coefficient is related to the absorption and scattering coefficients of the water in a way that is not completely understood, but depends on the field of view of the lidar. In an operational system, this parameter can be obtained directly from the lidar data. A very narrowly collimated system (defined as one whose field of view is much smaller than the average scattering angle in the water and much smaller than the ratio of the beam attenuation coefficient to the lidar height) will have an attenuation that is very close to the sum of the absorption and scattering. A wide field of view collects multiple scattered photons, and the attenuation is closer to the absorption coefficient.

The noise in a lidar system can come from several different processes. One of these is likely to predominate in any particular set of circumstances. One source is thermal noise in the receiver. This is an additive noise that is independent of signal level. It is Gaussian with zero mean. Another source is the shot noise from the sum of the signal current, background-light-generated current, and detector dark current. This is a Poisson process that depends on the total detector current. However, except for very low illumination levels, the Poisson distribution is nearly Gaussian, and we will make this approximation. Also, we note that if the signal from the fish school is very large, the detection probability is nearly unity, and accurate modeling of the

noise distribution is not critical. If the fish signal is small, the shot-noise variance will be very nearly the same whether fish are present or not. This is the situation that must be treated accurately, and so we can assume that shot noise can be approximated by a signal-independent, additive Gaussian process for the purposes of this paper. The final noise source is caused by variations of the optical properties of the water with depth. Variations that are slow compared with the depth resolution of the lidar can be estimated and eliminated. However, more rapid fluctuations will be indistinguishable from noise. In the absence of a better model for these fluctuations, we will also assume that they are Gaussian. Thus, an additive, signal-independent Gaussian noise will be considered, and the source of this noise will not be considered further. The final results will not be much different if the dominant noise is not Gaussian. Non-Gaussian noise will change the numerical values of the detection and false-alarm integrals. Because of the strong exponential decrease in signal level with depth, small changes in these values will correspond to small changes in detection depth. A similar effect is caused by our choice of threshold level, which also changes the detection and false-alarm integrals. We will show that the results are not very sensitive to our choice of threshold level for the same reason. It is possible that the variations in optical properties produce a highly non-Gaussian noise that will have a significant effect, but we have no evidence for this.

The probability density function (pdf) of the instantaneous signal (s) for a single pulse at some depth can therefore by approximated by a normal pdf with mean =S and variance = σ^2

$$f(s;S,\sigma) = \frac{1}{\sqrt{2\pi}\sigma}\exp\left[-\frac{(s-S)^2)}{2\sigma^2}\right] \qquad \textbf{(6)}$$

For illustration, we will assume that σ is not depth dependent, although S clearly is.

Detection is accomplished by setting a threshold signal level above which we will assert that fish are present. The detection probability is the probability that the instantaneous signal is above this threshold when fish are present (i.e., when $\beta_f > 0$). Thus,

$$P(DETECTION) = \int_T^\infty \frac{1}{\sqrt{2\pi}\sigma}\exp\left[-\frac{(s-S_f)^2)}{2\sigma^2}\right]ds, \qquad \textbf{(7)}$$

where T is the threshold level and S_f is the signal level with fish present. Specifying that fish are present whenever the received signal exceeds some threshold value entails some probability of a "false alarm." This probability can be calculated from

$$P(FALSE\ ALARM) = \int_T^\infty \frac{1}{\sqrt{2\pi}\sigma}\exp\left[-\frac{(s-S_w)^2)}{2\sigma^2}\right]ds, \qquad \textbf{(8)}$$

where S_w is the signal from clear water.

To reduce the number of free parameters, we can normalize everything by the noise level. Thus, we define a signal-to-noise ratio, $SNR = (S_f - S_w)/\sigma$ and a threshold-to-noise ratio $TNR = (T - S_w)/\sigma$. Then Equations (7) and (8) become

$$P(DETECTION) = \int_{TNR}^{\infty} \frac{1}{\sqrt{2\pi}} \exp\left[-\frac{1}{2}(s - SNR)^2\right] ds. \quad (9)$$

where s follows normal distribution with mean SNR and variance 1 when fish are present. and

$$P(FALSE\ ALARM) = \int_{TNR}^{\infty} \frac{1}{\sqrt{2\pi}} \exp\left[-\frac{1}{2}s^2\right] ds \quad , \quad (10)$$

where s follows normal distribution with mean =0 and variance =1 when no fish are present

The maximum detection depth, z_{max}, was defined as the depth at which the detection probability is 0.5, i.e., the SNR_z is equal to the TNR because of the sharp drop of detection probability from 1 to 0 with depth (Figure 2).

$$TNR = SNR_z = SNR_0 e^{(-2\alpha z)} \quad . \quad (11)$$

We can rearrange the terms in Equation(11) and calculate that

$$z_{max} \approx -\frac{1}{2\alpha} \ln\left(\frac{TNR}{SNR_0}\right). \quad (12)$$

We will investigate the degree that maximum detection depth for schools is affected by the setting of the false-alarm rate by calculating z_{max} as a function of the false-alarm probabilities and determine the value of TNR to be used in Equation (12). The detection probability (Equation(9)) can be approximated by unity for depths above this z_{max} and zero for depths below it (Figure 2). That is

P(DETECTION) =1 for SNRz>TNR or $z < z_{max}$
=0 otherwise.

2.05 Laser power and penetration depth:

To get an idea of the ranges of depths that might be available to the lidar for reasonable

cost, we calculated the maximum penetration depth with a lidar model that was developed to perform engineering trade-offs quickly and easily. Input parameters and lidar components can be changed quickly, and the computer program automatically calculates all of the affected quantities. Plots can be quickly generated within the program to allow the results to be immediately viewed. The lidar system was assumed to be similar to that currently used by NOAA (Churnside et al., 1997). Actual parameters are presented in Table 3.

Only laser power effects were considered. Clearly, other factors are also important. These include receiver telescope diameter, detector sensitivity, background light conditions, fish species and density, etc. However, a full investigation of the effects of all pertinent parameters was beyond the scope of this paper. The effects of some of these parameters can be estimated. Doubling the receiver telescope area, detector sensitivity, or fish density, for example, is equivalent to doubling the laser power, and we can consider an equivalent laser energy that includes differences in these parameters. Because of the assumptions used in these calculations, these numbers should be taken as representative and are not necessarily precise.

Because of the interference with the surface, it is difficult to actually calculate SNR_0. Instead, we note that

$$SNR_0 = SNR_z \exp(2\alpha z), \qquad \textbf{(13)}$$

where z is any arbitrary depth, and SNR_z is the signal-to-noise ratio at that depth. The calculations were actually done with a fish school deep enough so that the surface effects did not contribute. This equation does not hold for fish within about 1 m of the surface, but the errors are negligible for the depth distributions of fish used in this paper.

The signal and noise levels can be defined at any one of a number of points in the receiver, including optical power on the detector, current out of the detector, the voltage generated by that current through a standard 50 Ω resistance, the output of the log-amplifier, or the integer value that this produces when digitized. We will consistently use the voltage across 50 Ω, which is the input voltage to the log-amplifier. For an infinitesimally short laser pulse, this signal varies in time as the pulse propagates through the water. We can relate this time to the depth at which the light was scattered back to the receiver since we know the speed at which light travels through water. Therefore, we can write the signal as a function of depth as for a nadir-pointing:

$$S'(z) = \frac{P(z)\,\pi d^2 R\beta(\pi)}{4(z + nh)^2}\exp(-2\alpha z), \qquad \textbf{(14)}$$

where S' is the received signal per unit depth at depth z, P is the laser power, R is the responsivity of the detector and load in V/W, $\beta(\pi)$ is the backscatter coefficient of the water plus any fish present at that depth, h is the height of the aircraft above the surface, n is the index of refraction of water (1.33), and α is the lidar attenuation coefficient.

To get the actual signal voltage, we must integrate Equation (14) over the finite duration of the laser pulse. To get the short pulses desired, it is necessary to use Q-switching. In this

technique, the laser resonator is blocked electro-optically while the energy is stored in the lasing medium. The cavity is then quickly opened. Lasing begins rapidly, and the output power quickly builds to a high value. As the energy in the lasing medium is depleted, the output power decreases back to zero. This technique produces a characteristic pulse shape that can be approximated by

$$P(t) = \frac{Et}{\tau^2}\exp\left(-\frac{t}{\tau}\right), \qquad (15)$$

where E is the total pulse energy, and τ is 0.408 times the full width of the pulse at one half of its maximum value. We convert this time to distance through the speed of light, and integrate Equation(14) over depth.

Two water types were used. These are the Jerlov (1968) types IB and III. These specify only the diffuse attenuation coefficient K_D. To obtain an estimate of lidar attenuation we need to have an estimate of the volume scattering function $\beta(\theta)$, where θ is the scattering angle. We will use the general functional form of Petzhold (Mobley 1995; Petzhold 1972) with the exact values scaled by the value of the scattering coefficient inferred from the different values for K_D. We first note that

$$K_D = a + 2\pi b \int_{\frac{\pi}{2}}^{\pi} \frac{\beta(\theta)}{b}\sin(\theta)\,d\theta, \qquad (16)$$

where a is the absorption coefficient of sea water, b is the scattering coefficient, and $\beta(\theta)/b$ is the normalized scattering function of Petzhold. From this expression, we obtain the scattering coefficient and the backscatter coefficient for each of the Jerlov water types. The beam attenuation coefficient is given by

$$c = a + b. \qquad (17)$$

The lidar attenuation coefficient lies somewhere in between the diffuse attenuation coefficient and the beam attenuation coefficient in a way that depends on the beam divergence of the lidar and on the spot size at the surface. The details of this dependence are not completely understood, and we will make what we hope are reasonable estimates. Following Feigels and Kopilevich (1994), we estimate the divergence angle effect for a beam of negligible size by assuming that photons scattered at angles greater than the lidar divergence angle $\phi/2$ are lost. We then apply a correction to this value for the finite size of the spot at the surface based on a curve fit to the results of Gordon (1982). The final result is an estimate for the lidar attenuation coefficient given by

$$\alpha = K_D + 2\pi b \exp(-0.8c\phi h) \int_{\frac{\phi}{2}}^{\frac{\pi}{2}} \frac{\beta(\theta)}{b} \sin(\theta) d\theta, \qquad \textbf{(18)}$$

where h is the height of the lidar above the surface. The results are fairly sensitive to this parameter; a factor of 2 in α is equivalent to a factor of 2 in depth penetration. The values used in this paper are consistent with observations in the Southern California Bight, and are representative of what can be expected. However, more work is needed before accurate predictions of detection probability can be made for a specific water mass based on measurements of the optical properties. Direct measurements of α can provide better detection predictions, and can also be used to refine this relationship.

2.06 Vertical distribution and packing density of fish schools:

The vertical distributions of schools below the surface, their packing density and fish size are critical biological properties affecting detection of schools by a lidar. Two vertical distributions of epipelagic fish schools were used in our analyses. One represents an average distribution of epipelagic schools of small pelagic fishes during the day and another during the night (Figure 3). The daytime vertical distribution is a fit to the average of the May 1997 and September 1997 surveys of Holliday and Larson (1979), who used a bottom bounce acoustic propagation path technique which may sample the upper 10-20 m better than conventional acoustic methods. The night vertical distribution curve is a fit to the cumulative proportions of newly-spawned anchovy eggs from two California sites (Pommeranz and Moser 1987) and anchovy schools from three anchoveta acoustic surveys in Peru (Castillo V. 1995). The depth of early stage anchovy eggs may indicate school depth since they spawn during the night. Although the curves are based on anchovy data, we considered them to represent vertical distributions of sardines and herring as well. Whatever differences may exist between these species in southern California waters is masked by the great variability that exists within one species. Vertical distributions during the daytime and nighttime were fitted to an exponential distribution:

$$F(z)=p(Z<z)=1-\exp(-z/\lambda) \qquad \textbf{(19)}$$

where F(z) is the proportion of fish schools that is in the upper z meter depth and λ is the mean depth of the fish schools.

Direct measurements of school packing density (numbers/m^3) exist for two species of small pelagic fishes of interest in this study (Table 4). Graves (1977) deployed a dropped camera by day and Aoki and Inagaki (1988) used a tethered camera by night and obtained packing density of anchovy with average length of 10 cm. Freon et al. (1996) provide estimate of packing density for a sardine school (13 cm) in the Caltalan Sea Spain, using a dual-beam vertical echo-

sounder (BioSonics) connected to a school integrator software package (INES-MOVIES-B) which estimates school parameters in terms of size, geometry, and density. Freon et al. (1996) computed the target strength (TS) from the fish length using the equation by Foote (1987) for clupeoids (TS=20 logL-71.9; L=13). The fish density (Dv) was then computed from the back scattering volume (Sv) based on the equation: Sv=10 log (Dv) +TS. The fish density (Dv) during the night was 4 for Sv=-43.5 and during the day was 58 for Sv =-32 (Freon et al.1996).

We extend our analysis to larger epipelagic fishes such as herring and mackerel-like fishes by using data for 20 cm and 34 cm herring for the daytime only (Misund 1993). For 20 cm fish, we read packing density (5 fish m^{-3}) corresponding to fish length of 20 cm from Figure 4 of Misund (1993). For 34 cm fish we estimated the mean and standard deviation of 20 "cell-integrated" herring schools from Figure 6 of Misund (1993). We performed a lognormal transformation on the original observations of packing density for herring (34 cm) because the transformed data were closer to normal than the original data and the calculated means and standard deviations of the log-transformed data. Moreover, we believe that CV (=1.55) of the packing density for 34 cm herring was more realistic than the CV (=0.48) of 10 cm anchovy because the SD for herring measured the overall variation, whereas the SD for anchovy may only measure the variation among schools (Aoki and Inagaki, 1988). For modeling purposes, we computed the mean (μ_y) and variance (σ_y^2) of y=ln(x) where x is the packing density, for 10 cm anchovy, 13 cm sardine and 20 cm herring:

$$\hat{\sigma}^2_y = \ln[cv^2(x)+1] \quad , \qquad \textbf{(20)}$$

$$\hat{\mu}_y = \ln(\bar{x}) - \hat{\sigma}^2_y/2 = \ln(\bar{x}) - \ln(cv^2(x)+1)/2 \quad , \qquad \textbf{(21)}$$

where cv(x) of herring (= 1.55) was used. Equations (20) and (21) were derived from the following two relations: $\mu_x = \exp(\mu_y + \sigma^2_y/2)$ and $\sigma_x^2 = \exp(2\mu_y + \sigma^2_y)[\exp(\sigma^2_y) - 1]$.

Depth specific probability of detection ($p_a(z)$) based on packing density

As mentioned in an earlier section, P(DETECTION) =1 for SNRz > TNR and zero otherwise, because the steep drop of P(DETECTION) around z_{max} . The proportion of fish that can be detected and identified at depth z, $p_a(z)$, was modeled by the $P(SNR_z > TNR)$. The probability of detection ($p_a(z)$) was computed through the probability density function of fish packing density (x) at depth z, assuming the SNR_0 is proportional to the packing density(x), i.e. $SNR_0 = Ax$, where A is the proportionality and is a function of fish size and reflectivity. Assuming the reflectivity is the same for all fishes, then A is a function of fish size only, $A \sim 10^4 * L^2$ where L is the fish length in meters (Churnside et al. 1997). The packing density, x, is a lognormal random variable. We can write $SNR_z = SNR_0 \exp(-2z\alpha) = Ax \exp(-2z\alpha)$, thus, $SNR_z > TNR$ is equivalent to $x > (TNR/A)\exp(2\alpha z)$, and we approximated the proportion of fish detected at depth z based on lognormal distribution of packing density (x) by

$$p_a(z) = \int_{\exp(2\alpha z)TNR/A} p(x)dx$$
$$= p(\ln(x) > [2\alpha\ z + \ln(TNR/A)]) \qquad (22)$$
$$= 1 - \Phi\left(\frac{2\alpha\ z + \ln(TNR/A) - \mu}{\sigma}\right) \quad ,$$

where $\Phi(u) = P(U<u)$ for normal random variable, U, with mean=0 and variance =1 and ln(x) has mean μ and variance σ^2.

Equation(22) was computed through SNR_z, the mean of each individual normalized signal (or pulse). In appendix, we computed $P_a(z)$ through individual normalized signal (Equation(9)). This also assumes that the effects of shadowing can be neglected. While more work on this issue is needed, our results suggest that it is not a serious effect. We have observed multiple layers of fish in our data, suggesting that light is getting through the first layer. We have also observed the water return from below and above schools of fish and found that the additional attenuation caused by the fish is small compared with the background water attenuation.

Proportion of fish schools detected (q)

The proportion of fish schools detected in the upper z meters (q_z) depends on the depth specific probability of detection ($P_a(z)$; Equation(22)) and the vertical distribution of fish schools (Equation(19)). The quantity (q_z) was computed by numerical integration:

$$q_z = \int_0^z p_a(u) f(u) du$$
$$= \int_0^z \left[1 - \Phi\left(\frac{2\alpha\ u + \ln(TNR/A) - \mu}{\sigma}\right)\right] \frac{1}{\lambda} e^{-\left(\frac{u}{\lambda}\right)} du \quad , \qquad (23)$$

where $p_a(u)$ is from Equation(22) and $f(u)$ is the exponential pdf from Equation(19):

$$f(u) = \frac{1}{\lambda} e^{-\left(\frac{u}{\lambda}\right)} \quad . \qquad (24)$$

The quantity, q_z, increases with the depth z and reaches an asymptote at z_{max} (q; q<=1) and q is defined as the proportion of fish schools detected.

2.07 Criterion for evaluating trade-offs between penetration depth and swath width

If laser power were held constant, increasing the swath width would decrease the maximum depth of penetration of the laser pulse. In this section, we establish a criterion for comparing various instruments having different combinations of swath width and laser power (maximum

penetration depth). The effectiveness of the width of a swath (y) can be measured by the probability that fish schools will be encountered (p_y) in the swath (Equation(1) or (2) from simulation). The effectiveness of a lidar in detecting schools within the swath is measured by the proportion of fish schools detected (q) (Equation(23)). The product of p_y q (Equations 1 or 2 and 23) was then used to evaluate the overall effectiveness of any instruments with a given swath width (y).

3. RESULTS

3.01 Effects of Swath Width on Encounter Probability

Considering first the relatively simple case of randomly distributed schools along a single transect or swath, we used a simple encounter model (Equation(1)) to calculate the probability of encountering schools for swath widths ranging from 1-1600 m. In this example, we considered schools of 30 m and 150 m diameter and population sizes of 10 to 5000 schools in the surveyed area (42,204 km^2). The effect of increasing swath width on encountering schools was most pronounced when the swath width increased from 10 m to 200 m (Figure 4), for a population which consisted of many small schools (over 1000 schools with diameters =30 m) (Figure 4a), or a population which consisted of a moderate number of large schools (between 300 -1000 schools with diameters= 150 m) (Figure 4b). At low school densities, 10 to 50 schools in the survey area encounter probability changed gradually with swath width due to the rarity of schools. Obviously if the number of schools is constant, the probability of encountering large schools (150 m) is higher than that of small ones (30 m).

When multiple swaths are considered, the probability that at least one of them intercepts a fish school (Equation(3)) increases with school diameter, number of schools, and number of transects. This probability is most sensitive to the swath width and number of swaths when the number and diameter of the schools are small (Table 5). For example, to guarantee an encounter probability ($p_{y,n}$) of at least 0.5 (Equation(4)), would require 25 transects of swath width < 1 m, or 5 transects of swath width >=200 m when the population size is 300 schools and the school diameter = 30 m. On the other hand, if population size were 1000 anchovy schools (approximate biomass 12,000[5] mt), only 5-10 transects of swath width < 1 m would be required. When the school diameter is 150 m, five transects of any swath width will guarantee more than a 50% chance that some transects will intersect some fish schools. Thus, the width of the swath width becomes unimportant for schools of large diameter.

We now consider the more complex case of schools being aggregated into school groups rather than being randomly distributed. When schools were aggregated into school groups and the school diameters and densities were equal to or greater than those reported by Smith (1981), then

---

[5]12 mt/anchovy school =115 fish /m^3 * (30 m/2)^2 * 3.1416 * 10 m (depth)* 15 g/fish* 1 mt/1000000 g where 115 fish/m^3 is the packing density and 30 m is the average diameter of a fish school.

swath width had little effect on the probability of encountering schools. This was true for all three population sizes (Figure 5). Encounter probability was affected by the swath width only when the diameters of school groups were small and the school density within the school group was so low (multipliers of 0.5) that their distribution became nearly random rather than aggregated. In these cases, the encounter probability increases sharply when the swath width increases from 1 m to 50 m. Even this very limited effect of swath width diminishes as the number of schools in the survey area increases. The encounter probability for swath widths greater than 50 m is almost a constant regardless of the conditions.

For the multiple swaths, the probability that at least one of them intercepts a fish schools (equation (3)) was much higher for aggregated fish schools than random distributed schools. The lowest probability was 0.65 for the case where fish were aggregated in few large school groups and the population was low, i.e. 16,000 (1.5,1.5) for n=5 (equation (3)). For n=10, the probability ($p_{y,n}$) was close to one for all cases.

3.02 Depth-Specific Detection Probability

The depth at which a lidar will detect a school or target will depend in part on the threshold setting of the instrument relative to the noise (TNR). To illustrate these relationships we fixed a false alarm rate for the detection of schools, used an alarm rate to determine the threshold level (Equation(10)), and then calculated the detection probability for schools (Equation(9)). The results of such a calculation are presented in Figure 6, where the detection probability for fish schools is plotted as a function of the probability of a false alarm for signal-to-noise ratios of 1 and 3. Zero, the lower limit of the plot, corresponds to a very high threshold (TNR) setting, where the probability of a false alarm and the probability of detecting a school are both zero. At a setting of zero we would conclude that fish are never present. The upper limit of Figure 6 corresponds to a very low threshold setting, where P(false alarm) and P(detection) are both unity; at a setting of 1 we must conclude that fish are always present.

If one selects a reasonable false-alarm rate and a signal-to-noise ratio at the surface, one can calculate the detection probability as a function of depth (Equation(9)). This was done for a false-alarm probability of 1% and a lidar attenuation coefficient of 0.1 m^{-1}, and the results are plotted in Figure 2 for several values of the surface signal-to-noise ratio. There are several interesting features of these results. The first is that when a critical depth is reached, the detection probability drops abruptly from nearly unity to nearly zero over a narrow, 5-10 m span of depth. Because of this sharp transition, we can define as maximum detection depth z_{max} as the depth at which the detection probability is 0.5. The depth, z_{max}, depends logarithmically on signal level because of the exponential attenuation of the signal with depth. Thus, each order-of-magnitude increase in signal level (illustrated in Figure 2) provides an increase in z_{max} of just over 10 m in depth. *Ten m* is just about 1 lidar attenuation depth, defined as α^{-1} (Equation(12)). We can rewrite Equation(12) as $z_{max} = \ln(SNR_0/TNR) * 0.5 * \alpha^{-1}$. Therefore, if the attenuation coefficient (α) is different from 0.1 m^{-1}, the value used here, these z_{max} depth values scale linearly with lidar attenuation depth (α^{-1}).

To examine the sensitivity of z_{max} (Equation(12)) to TNR and thus the false alarm probability (Equation(10)), we used the same values of the surface signal-to-noise ratio as those used in Figure 2. This calculation indicated that the maximum detection depth (z_{max}) was relatively insensitive to changes in false-alarm probabilities. Decreasing the false alarm rate by a factor 10

from 0.01 to 0.001 would only increase the maximum detection depth by a few meters (Figure 7). Thus, a fairly low rate of false alarms for a system can be selected without seriously degrading the detection performance. It also implies that we can select a nominal threshold level and obtain a simple expression for the maximum detection depth. A value of $TNR = 3$ results in a false-alarm probability of just above 0.1%. Therefore, according to Equation(12), z_{max} is determined by

$$z_{\max} \approx -\frac{1}{2\alpha}\ln\left(\frac{3}{SNR_0}\right). \qquad (25)$$

We now consider the depth in the sea at which schools may be detected by a single lidar pulse and compute, using Equation (22), the proportion of fish schools that would be detected for each of our examples (Figure 8). During the daytime, and at a depth of 30 m, 97% of schools of 10 cm anchovy, 98% of 13 cm sardine, 46% of 20 cm herring, and 51% of 34 cm herring schools would be detected (($p_a(z)$, when $\alpha = 0.1$). Moreover, one can also compute signal-to-noise ratio from the packing density(x): $SNR_z = A \times \exp(-2\alpha z)$ for fish length between 10 and 34 cm and compare it to the threshold target-to-noise ratio (TNR) of 3. At the surface, SNR_0 was 11,480 for 10 cm anchovy, 9,802 for 13 cm sardine, 2,000 for 20 cm herring and 2971 for 34 cm herring. At a depth of 30 m SNR_{30} ($\alpha = 0.1$) for these cases were 28.5 , 24.3, 4.96 and 7.36, respectively. All the SNR_z were above TNR =3 indicating most of the schools in the upper 30 m will be detected. The SNR_z for anchovy was much higher than the other species because the packing density of anchovy was much higher than other species (Table 4). The detection probability for anchovy was unity over the upper 30 m (Figure 2), which was consistent with the results computed from Equation(22) (Figure 8).

During the night, the packing density is much lower (0.53 anchovy/m^3 and 4 sardines/m^3) but the signal-to-noise ratio at the surface (SNR_0) for these schools was 53 for the very diffuse groups of anchovy and 676 for the more compact schools of sardine, both values being substantially above a TNR of 3. At 20 m, the SNR_{20} for anchovy schools declined to 0.97 with a probability of detection of only 13%, while the SNR_{20} for sardine, because of their higher nighttime packing density (in our example), was higher(12.38) and the probability of detection at 20 m was 77%. At 30 m, the detectability of anchovy was less than 1% while it was 14% for sardine.

3.03 Overall vulnerability to lidar of schools in the vertical plane

In this section we estimate the cumulated proportion of schools of anchovy, sardine, and herring that might be detected by a lidar assuming constant day and night vertical distributions. As the first step in this discussion, we focus on the two components used to make the estimate: the average vertical distributions of schools of pelagic fishes during the day and the night (Figures 3 and 8) (Equation (19)); and the depth specific probability of detecting a school, which was discussed in the previous section (Equation(22)). These two components are combined to obtain the final estimates

Our analyses were based on the average day and night vertical distributions of anchovy schools, because the distributions were very similar to those of many other epipelagic schooling

fishes such as mackerels and sardines (Castillo V. 1995), with about half of the schools occurring above 30 m during the day and about 90% during the night. Specific differences may exist in the vertical distribution of schools, but such trends are masked by the high variability that exists between cruises for a species. By associating these two general vertical distributions with published field measurements of packing density, we produced six examples of school conditions, two during the night (10 cm anchovy and 13 cm sardine) and four during the day (10 cm anchovy, 13 cm sardine, and 20 cm and 34 cm herring).

In general, the probability of detecting a school during the day declined slightly from about 1 at the surface to 0.95 at 25 m, and approached zero at 45-50 m. No major differences existed among our day examples, since these schools were relatively compact and the detection function is driven largely by the lidar attenuation coefficient (α =0.1, Equation(22)) (Figure 8). The depth specific probability of detecting a school was much lower during the night than during the day. However, distinct differences existed between sardine and anchovy in their night-time detection probabilities. At a depth of 25 m, the probability of detecting sardine at night dropped from the daytime value of 0.92 to a night probability of 0.40. The day-night change in anchovy was more marked, with the detection probability dropping from 0.95 to 0.10. Detection probabilities were lower during the night because packing densities were lower. Similarly, anchovy schools were less detectable during the night than sardine schools because they were more diffuse. It is unlikely that the observed differences in night packing density between anchovy and sardine examples are due to species differences since anchovy also form distinct and highly aggregated schools during the night(Squire 1972) as well as the more diffuse aggregations measured by Aoki and Inagaki (1988). One of the more important aspects of these results was that even the very diffuse nighttime aggregations of anchovy (0.53 fish/m^3) (Aoki and Inagaki 1988) can be distinguished from background noise. That shallow nighttime schools can readily be detected by an airborne lidar despite their low packing density means during the night lidar surveys are feasible.

By combining the detection probabilities with the vertical distributions, we can calculate the proportion of schools detected (q) by the lidar for each of our six examples (Figure 9). This calculation indicates that a night lidar survey would be more accurate than one during the day as the cumulated proportion of schools detected during the night is higher regardless of fish size and packing density. If the fish have a relatively high packing density during the night, as did the 13 cm sardines in our example, we could expect to detect about 80% of the schools. If the night schools were very diffuse, as was our anchovy example, our model predicts that about 60% of the schools would be detected during the night. During the day, schools of 13 cm (sardine), 20 cm (herring), and 34 cm fish (herring) were not detected below about 40 m due to their lower packing density while anchovy (10 cm) with a much higher packing density (115 fish m^3) were detected down to about 50 m.

Up to this point we have discussed only cases in which the lidar attenuation coefficient, α , equals 0.1/m, a typical value for the coastal waters of southern California. To illustrate the effect of water clarity, we varied α from 0.05 to 0.6, where the attenuation coefficient for the dirtiest coastal water was 0.52. We computed the proportion of schools that could be detected (q) in each of our six examples. We plot these data as a function of the signal-to-noise-ratio at the sea surface (SNR_0), which is a function of only the fish size and packing density (Figure 10). The proportion of schools that could be detected declines rapidly with increasing α which depends on details of the lidar as

well as the properties of the water, but several generalizations can be made. During the night the lidar field of view can be large because there is less background light to interfere with the signal. Under these conditions, the lidar attenuation coefficient will be very nearly equal to the diffuse attenuation coefficient. For the Jerlov open-ocean-water types at the typical 532 nm wavelength, this varies from about 0.05/m (Type I) to about 0.11/m (Type III). The values for the Jerlov coastal water types range from 0.15 (Type 1) to about 0.53 (Type 9). From Figure 10, we expect that most schools will be detected during the night in the open ocean.

During the day, the situation is more complicated. A lidar system with a large field of view will have a smaller signal-to-noise-ratio during the day because of scattered sunlight reaching the receiver. We can increase the signal to noise by decreasing the field of view, but this tends to increase α. Also, from Figure 10, we see that increasing the signal-to-noise-ratio during the day has little effect on the proportion of schools that could be detected, even though during the night such changes have important consequences, because the day and night vertical distributions of schools are different. The day distribution has a maximum 20 m but a long tail extending down to 155 m (Castillo V. 1995), while during the night, 82% of the schools are in the upper 20 m. Thus, an increase in the signal strength that extends the maximum depth of a return by 10 m or so could have an important consequence during the night but a trivial one during the day. This argument, of course, assumes some minimal signal-to-noise-ratio (e.g. $z_{max} > 20$ m) to begin with.

We can summarize the main differences between night-and daytime operation as follows: During the night, solar background is not a problem, and we expect the fish to have a shallow distribution. We can operate with a wide field of view and obtain the minimum value of α with no signal to noise penalty. The detection probability is high, and the fish size and packing density will have a considerable effect on the total proportion of schools detected. During the day solar background is a problem, and we expect the fish to have a deeper distribution. We will likely have to decrease the field of view to obtain an acceptable signal-to-noise-ratio, which will increase α. However, once an acceptable level of signal to noise is reached, a further increase has little effect on the total proportion of schools detected. The detection probability during the day is lower than during the night, and fish size and packing density have a much smaller effect on the total proportion of schools detected. Finding the right balance of signal-to-noise-ratio and α for daytime operation is a problem that remains to be solved.

3.04 Comparisons with vision-based methods

In this section we compare the ability of a visual observer to count fish schools with that of a lidar. Hara (1990) reported that a visual observer flying at 500 m will be able to detect sardine schools along a 1600 m swath and to a depth of about 4 m. We assumed all schools at 4 m are detected visually and none are detected below that depth. For the lidar, we used a swath width of 7 m, and we considered the product of encounter probability (p_y) (Equation(2)) depicted by swath width and the maximum proportion of schools detected (q) depicted by depth (Equation(23)) to be a measure of the overall performance.

A visual observer detects somewhat more schools in the horizontal plane than does a lidar because of the relatively large swath width of a visual observer (Table 6). The encounter probabilities in the horizontal plane, (Equation(2)) obtained from simulation for a population of 32000 schools was 0.51 for visual observation and 0.42 for the lidar. In the vertical plane, however,

our analysis demonstrates the superior ability of a lidar to detect schools both during the day and during the night. During the night, proportion of fish schools detected (q) for the lidar varied from 0.52 to 0.84 depending on fish size and packing density, while it was 0.28 for the visual observer. The difference between visual and lidar systems was much greater during the day, since q for all six school examples during the day was at least 0.53 for the lidar, while that for the visual observer was only 0.095.

The $p_y q$ (an overall measure of detection performance) for a lidar was at least 1.9 times that of a visual observer. This means on the average, a lidar would be about twice as efficient as it would be for a visual observer in detecting fish schools during a survey.

We have considered here, however, only one aspect of the two systems - the detection rates. Many other differences also exist relating to species identifications, biomass, and effects of environmental conditions on the observing system.

3.05 Laser Power and Penetration Depth

A set of parameters used to compute the laser power and penetration depth for schools of sardines are listed in Table 3. The lidar signal was computed using Equation (14) and the penetration depth was computed based on the attenuation coefficient estimated by Equation(18). The relation of penetration depth and the logarithmic laser energy for both open ocean and coastal waters was obtained (Figure 11). Calculations of SNR_0 were made at two laser power levels, and the logarithmic dependence was used to generate the curves.

We calculated the maximum penetration depth for the NOAA lidar, with a power of 67 mJ, and scaled that depth with laser power. For this calculation, we assumed 13 cm sardines with a packing density of 4 m^{-3} (Table 3). Night flights at 100 m altitude were assumed. Two water types were used, one typical of open ocean water (Jerlov Type IB) and one more typical of coastal water (Jerlov Type III) (Jerlov 1968).

The current NOAA lidar is capable of operating from a single-engine plane, which weighs about 100 kg and requires less than 1 kW of power. The cost of the components was about $50K. The penetration depth for this system under these somewhat optimum conditions is estimated to be about 45 m (Figure 11). Some cost can be saved by going to a lower-power laser and smaller telescope, but not a great deal. A savings of only about $10K is likely even if one goes to an equivalent energy of 1 mJ. This still provides about 35 m of depth penetration for the conditions assumed here.

On the other end, one can obtain 60-65 m penetration by going to a system with equivalent pulse energy of 100 J (Figure 11). However, this would be a very large expensive system. Part of the equivalent energy could be obtained by using a larger telescope, but only a little over an order of magnitude. This still implies a laser pulse energy of 10 J. This is a custom laser, with a cost that we estimate to be in the order of one million dollars. In addition, it would require something in the order of 100 kw of power, which cannot be supplied by a small, single-engine aircraft. An aircraft something like the DeHaviland Twin Otter may be necessary to accommodate the size and power requirements of this system. The system size and cost probably increase significantly at an equivalent energy of about 1 J, so a practical range of penetration depths is probably between about 40 and 60 m.

4. DISCUSSION

Our goal was to model various aspects of a lidar survey system for epipelagic fishes with a focus on features that might affect survey precision and accuracy. We learned from our modeling of swath width that the width would have little or no effect on the rate schools are encountered when they are aggregated into school groups, as is commonly the case for sardines and anchovy, except under very low biomass levels. Under conditions of very low biomass, schools may become scattered rather than aggregated, in which case encounter rates would increase with swath width. Our analyses also showed that the chance that all the transects do not intercept any fish school was extremely small because number of transect lines is likely to be much more than 5, due to the high speed of airplane. Thus, from the standpoint of survey precision swath, width may be given a low priority.

Lack of full vulnerability to the counting technique is one of the most important potential sources of bias for biomass surveys. Fish may not be fully vulnerable because the survey does not extend over the full geographic range of the stock, and because of the limitations of the counting system. Nearly all fishery-independent surveys suffer to some extent from these problems. In the case of an airborne lidar survey, the depth limits of the sensing system could produce a large potential bias, particularly if the system is used during the day. Our model indicates that on the average 46% of daytime schools of small pelagic fishes would be expected to be below the maximum detection depth of the lidar (30 m). As the vertical distribution of schools can vary considerably between surveys, the undetected fraction would vary, thus affecting survey accuracy. This computation is driven by our daytime vertical distribution curve and the rapid attenuation of light in water, and packing density and fish size have negligible effects. Thus, reliable estimation of the biomass of such small schooling fishes during the day in offshore waters does not seem practical unless a reliable unbiased estimate of vertical distribution of schools is available. On the other hand, on the shelf in water up to 30 m depth, accurate daytime estimates are practical because the vertical movements of the fish would be restricted.

If a lidar survey were restricted to night flights, when schools are closer to the surface, the bias caused by the uncounted fraction of deep schools would be considerably reduced. During the night, however, schools may become very diffuse and consequently have a much lower target strength which affects their detectability. The good news from our modeling work was that even the very diffuse night schools of 10 cm Japanese anchovy (0.53 m^{-3}, Aoki and Inagaki 1988) are detectable over the upper 20 m. Our model indicated that 65% of all anchovy schools and 84% of all sardine schools would be detected during the night. The difference between anchovy and sardine examples is due to the higher packing density used in the sardine example (4 fish/m^3). During the night, packing density becomes an important variable because of the shallow vertical distribution of schools. In theory, packing density, and consequently lidar target strength, should decrease with increasing fish size (L) because the packing densities of schools change in proportion to L^{-3} (Misund 1993) while the reflective area increases with fish size in proportion to L^2. However, the average relationship between packing density and fish size is of less importance during the night because of the huge range in packing density of schools observed during the night. The density of schools during nighttime vary from compact schools suitable for capture by the commercial purse seine

fishery (Squire 1972) to schools so diffuse that many authors have concluded that schooling ceases (Whitney 1969; Blaxter and Hunter 1982). The packing density used in our example of anchovy during the night provided by Aoki and Inagaki (1988) represents the diffuse school state; we have no direct measurements of more compact night schools of anchovy. If the average packing density of anchovy were higher, which we believe is likely, then a greater proportion of anchovy schools would be detected during the night. If 85% of all schools were detected during the night, as the sardine example illustrates, night aerial lidar surveys could provide useful estimates of the biomass for anchovy as well as for sardine.

Detection of schools during the night would improve if maximum schooling depth and α were correlated as Hunter and Nicholl (1985) speculate. They determined the visual threshold for schooling in northern anchovy ($6 * 10^{-11} W\ cm^{-2}$) and suggested that the maximum nighttime depth was a function of the fishes ability to see one another. They estimated that the visual threshold for schooling would occur at 38 m during a full moon and at 30 m on a starlit night where chlorophyl was 0.2 mg Chla m^{-3} and at 8 m (starlit) and 20 m (full moon) when chlorophyl was 2.0 mg Chla $^{-2}$. If Hunter and Nicholl (1985) are correct, then the maximum lidar detection depth should increase with increases in the maximum night schooling depth, as long as flights are made under the same moon phase. This also indicates that it may also be important to exclude survey nights having a full moon, a rule long observed by the pilots who locate schools for the fishing industry.

It may be possible in practice to detect schools somewhat deeper than our model indicates because the model estimates the detection of a single pulse at one range gate or depth. In practice, a lidar will generate a composite image of a school derived from a number of such pulses over a range of gates (depths) analogous to an echogram trace (Figure 12). Such a composite image produced from multiple returns and gates can be more readily separated from background noise than a single pulse, but this involves a more complex, and at the present time, somewhat qualitative discrimination process. Signal-processing algorithms can be developed for this application, but their performance will depend on the exact algorithm used. More accurate estimates of detection depth depend upon the development of such signal-processing algorithms. Development of detection algorithms is one of the most promising directions for future research on fisheries lidar. Their development would greatly improve both the precision and accuracy of future lidar surveys for fisheries as well as reducing the work in processing the images. Similarly, improved knowledge on the causes for the observed variation in the vertical distribution of fish could improve survey precision and accuracy. The phase of the moon, time of day, mixed layer depth, temperature, location of forage, fish size, season, spawning habitats, may all influence where in the water column a school may be found.

It does not seem likely that it will be possible to greatly improve the depth of detection by increasing sensitivity or power of the lidar system over the basic radiometric system used in our model. Our analysis indicated that an order of magnitude increase in equivalent laser power (laser power plus sensor changes) would gain about 10 m in detection depth. Such a change would require a custom rather than off-the-shelf laser costing around a million dollars, plus associated costs including a larger aircraft to satisfy the new power and weight requirements. In addition, increasing the depth of penetration by 10 or 20 m, on the average, will not increase the numbers of schools detected by more than about 10% in daytime since school distributions tend to be skewed with a long tail extending to depths far beyond the practical limits of lidar in coastal waters. A 10 m gain would be more significant during the night but may not be worth the additional cost.

Up to this point in our discussion, we have treated the failure of a lidar to count deep schools as a potential bias. This is true unless an unbiased estimate of the mean vertical distribution of schools exists for the particular survey region and season and an appropriate statistical model is used for the survey. When these conditions are met, the failure of a lidar to count deep schools becomes a matter of precision rather than bias. An unbiased estimate of the mean vertical distribution of schools could be estimated from data generated by lidar and acoustic surveys for the same region, since by combining the two surveys one corrects for the vertical bias in each. The appropriate statistical model for a lidar survey would be one based on line transect theory (Buckland et al. 1993). Line transect theory usually deals with encounter rates on the horizontal plane assuming animals are uniformly distributed in space. In the case of lidar, we turn the model on its side. We use an average vertical distribution of fish schools in the survey area. An empirically derived vertical distribution does not seem to be subject to any more bias than the assumption of a uniform horizontal distribution, which is common practice in the line transect surveys.

For a line transect survey, the estimator for the population density is n/(2 L w P), where n is the observed animal count or biomass from the platform, L is the total length of transect lines, w is the transect width and P is the proportion of animals observed in the area within the width w and $P=\int_0^w g(x)f(x)dx$ where f(x)=1/w. The detection probability, g(x), is a decreasing function of the distance of animals from the line with g(0)=1. For a lidar survey, signals of fish schools collected along the transects from the water column decrease as the depth increases. The estimator of population density can be written as n/(2 L w q), where q (Equation(23)) is the maximum proportion of fish schools detected. The value, $q=\int_0^\infty p_a(x)f(x)dx$, depends on the attenuation coefficient (α), and the vertical distribution of fish schools (f(x)). The detection probability, $p_a(x)$, is analogous to g(x) in line transect survey, and f(x) in our examples is an exponential. In a lidar survey, and q may vary among transects, then a ratio estimator like $\frac{\sum n_i/q_i}{\sum 2L_i w}$ may be more appropriate.

The precision of a line transect lidar survey shall depend, to a large extent, on the variation about the mean vertical function for fish schools, f(x), and the proportion of all schools that are beyond the reach of the lidar. Clearly, as the vertical distributions are quite variable, the smaller the uncounted vertical fraction the better, hence night flights still seem preferable to day. As a strategy for calibration one may wish to consider selecting survey conditions that might yield the lowest variation in vertical distribution considering such variables as season of the year moonlight, thermocline, and forage depth.

To provide indices of relative abundance based on airborne lidar is an important fishery application less demanding than estimating biomass. For an index of abundance, the extent schools are available for counting is not a major concern. Lidar seems uniquely well-suited for taking an inventory of the juveniles of small pelagic fishes (pre-recruits) because they are extremely patchy and tend to be in shallow water near the coast in areas difficult to sample with a research vessel. Lidar surveys can provide useful indices of adult biomass as well. Aerial observations (Lo et al.

1992) and passive imaging (Nakashima 1990; Nakashima and Borstad 1993) from aircraft are currently used in several fisheries as indices of the abundance of small pelagic fishes and a lidar-based system would have several advantages over these passive methods. Our computation using a deterministic model showed that a lidar survey may be about twice as efficient in detecting schools as a vision based system during the night and five times more efficient during the daytime, due to the fact that fish are in deep water during the day. During the nighttime a lidar will see more schools, but the difference is not huge because the very wide swath width (1600 m) of our hypothetical aerial observer compensated, to some degree, for the observer not seeing further beneath the surface. Lidar images can also be better quantified than those based on visual observers or cameras, since the school volume rather than school area can be estimated, thereby improving the precision of the index. In addition, detection is less dependent on sea state and is little affected by sun angle and can be carried out at any time of day. On the other hand, skilled aerial fisherman identify species of schooling fish with remarkable accuracy, while a remote species identification algorithm for a lidar will be difficult, if not impossible, to develop. After 50 years of hydro-acoustic research, securing voucher specimens by trawling is still the only method for identifying acoustic targets with certainty. The lesson to be learned from hydro-acoustics is that for species identification to be a reality in lidar surveys, additional sensing systems will be needed. That humans can make such distinctions visually provides the hope that species identification may be possible by combining lidar with passive imaging systems.

5. APPENDIX

The detection probability by depth ($p_a(z)$) was defined as the proportion that the mean values of SNR_z exceeds the threshold, TNR (Equation(22)).Strictly speaking, one should define the detection probability as the expected probability that each signal exceeds the threshold. The expectation would be computed by integrating over the pdf of mean SNR_z. For a lognormal distribution of mean SNR_z, we would have

$$P_a(z) = \int P(s>TNR|SNR_z)\,lognormal(SNR_z)\,dSNR_z$$
$$= \int_0^\infty [1-\Phi(TNR-SNR_z)] \frac{1}{\sqrt{(2\pi)}\sigma_s\ SNR_z} \exp(-0.5(\frac{\ln(SNR)_z-\mu_s}{\sigma_s})^2 d(SNR_z) \quad , \qquad (26)$$

where s is the signal-noise-ratio which follows normal (SNRz, 1) (Equation(9)) and SNRz is a lognormal random variable with mean : $\mu_s = \ln(A) + E(\ln(x)) - 2\alpha\ z$ and standard deviation σ_s = SD(ln(x)) where x is the packing density. Our exercise indicated that both detection probabilities from Equations (22) and (26) were very similar . Therefore Equation (22), although an approximation, was used in our computation because of its simplicity.

6. LITERATURE CITED

Aoki, I. and T. Inagaki. 1988. Photographic observations on the behaviour of Japanese anchovy *Engraulis japonica* during the night in the sea. Mar. Ecol. Prog. Ser. 43:213-221.

Blaxter, J.H.S. and J.R. Hunter. 1982. The biology of the clupeoid fishes. *In* Advances in Marine Biology, Academic Press, New York, 20:1-223

Buckland, S.T., D. R. Anderson, K.P. Burnham and J. L. Laake. 1993. Distance Sampling: Estimating abundance of biological populations. Chapman & Hall. London, Glasgow, New York, Tokyo, Melbourne, Madras. 446p.

Castillo Valderrama, P.R. 1995. Disribucion de los principales recursos pelagicos durante los veranos de 1992 a 1994. Instituto Del Mar Del Peru, Informe No 114.

Churnside, J.H. and J.R. Hunter. 1996. Laser remote sensing of epipelagic fishes. *In* Laser remote sensing of natural waters: from theory to practice, V.I. Feigels and Y.I. Kopilevich, eds. SPIE, Bellingham, Washington, p. 38-53.

Churnside, J.H., J.J. Wilson, and V.V. Tatarskii. 1997. Lidar profiles of fish schools. Appl. Opt. 36:6011-6020.

Cram, D.L. and I. Hampton. 1976. A proposed aerial/acoustic strategy for pelagic fish stock assessment. J. Const. Int. Explor. Mer. 37(1):91-97.

Eberhardt, L.L. 1978. Transect methods for population studies. J. Wildl. Manage. 42(1):1-31.

Feigels, V.I. and Yu.I. Kopilevich. 1994. Applicability of lidar remote sensing methods for vertical structure investigation of ocean optical properties distribution. *In* Ocean Optics XII, J. Jaffe, ed. Proc. SPIE 2258:449-457.

Fiedler, P.C. 1978. The precision of simulated transect surveys of northern anchovy, *Engraulis mordax*, school groups. Fish. Bull., U.S. 76(3):679-685.

Foote, K.G. 1987. Fish target strengths for use in echo integrator surveys. J. Acoust. Soc. Am. 82:981-987.

Fréon, P., F. Gerlotto and M. Soria. 1996. Diel variability of school structure with special reference to transition periods. ICES J. Mar. Sci. 53:459-464.

Gordon, H.R. 1982. Interpretation of airborne oceanic lidar: effects of multiple scattering. Appl. Opt. 21:2996-3001.

Graves, J. 1977. Photographic method for measuring spacing and density within pelagic fish schools at sea. Fish. Bull., U.S. 75:230-234.

Gunderson, D.R. 1993. Surveys of fisheries resources. John Wiley & Sons, Inc., New York, 248 p.

Hara, I. 1990. Comparison of ship and aerial surveys of sardine schools. IEEE Trans. Geosci. Remote Sens. 28(4):693-695.

Holliday D.V. and H.L. Larsen. 1979. Thickness and depth distributions of some epipelagic fish schools off southern California. Fish. Bull., U.S. 77(2):489-494.

Hunter, J.R. and J.H. Churnside, eds. 1995. Airborne fishery assessment technology - a NOAA workshop report. SWFSC Admin. Rep., La Jolla, LJ-95-02, 33 p.

Hunter, J. and R. Nicholl. 1985. Visual threshold for schooling in northern anchovy *Engraulis mordax*. Fish. Bull., U.S. 83(3):235-242.

Jacobson, L.D., N.C.H. Lo, and J.T. Barnes. 1994. A biomass-based assessment model for northern anchovy, *Engraulis mordax*. Fish. Bull., U.S. 92:711-724.

Jerlov, N.G. 1968. Optical Oceanography. Elsevier, Amsterdam, 194 p.

Lo, N.C.H., I.D. Jacobson, and J.L. Squire. 1992. Indices of relative abundance from fish spotter data based on delta-lognormal models. Can. J. Fish. Aquat. Sci. 49:2515-2526.

Mais, K.F. 1974. Pelagic fish surveys in the California Current. Calif. Dept. Fish Game, Fish. Bull. 162, 79 p.

Misund, O.A. 1993. Dynamics of moving masses: variability in packing density, shape, and size among herring, sprat, and saithe schools. ICES J. Mar. Sci. 50:145-160.

Mobley, C.D. 1995. The optical properties of sea water. *In* Handbook of Optics, Second Edition, M. Bass, ed. McGraw-Hill, New York, Vol. 1, Chap. 43, p. 36.

Nakashima, B.S. 1990. Capelin school surface area index for NAFO Div. 3L during the 1989 spawning season. Northwest Atlantic fisheries Organization SCR Do. 90/59, Serial No. N1780.

Nakashima, B.S. and G.A. Borstad. 1993. Detecting and measuring pelagic fish schools using remote sensing techniques. ICES Report C.M. 1993/B:7, Session T, Fish Capture Committee, 18 p.

Petzhold, T.J. 1972. Volume scattering functions for selected ocean waters. SIO Ref. 72-78, Scripps Inst. Oceanogr., La Jolla, 82 p.

Pommeranz, T. and H.G. Moser. 1987. Data report on the vertical distribution of the eggs and larvae of northern anchovy, *Engraullis mordax*, at two stations in the Southern California Bight March-April 1980. U.S. Dept. Commer., NOAA Tech. Memo., NOAA-TM-NMFS-SWFC-75, 140 p.

Smith. P.E. 1981. Fisheries on coastal pelagic schooling fish. *In* Marine fish larvae. Morphology, ecology and relation to fisheries, R. Lasker, ed. Washington Sea Grant Program, University of Washington Press, Seattle, 1-31 p.

Squire, J.L., Jr. 1972. Apparent abundance of some pelagic marine fishes off the southern and central California coast as surveyed by an airborne monitoring program. Fish. Bull., U.S. 70:1005-1019.

Whitney, R.R. 1969. Schooling of fishes relative to available light. Tran. Am. Fish. Soc. 98(3): 497-504.

7. FIGURES

1. A spatial distribution of school groups from one simulation run. Circles indicate areas covered by school groups for a population of 80000 schools. This graph was generated from lognormal distributions with mean =3.91 and variance=0.51 for school density and lognormal distribution with mean=2.319 and variance=0.676 for diameter of school group. G1, G2, G3 and E are the gaps used to compute the encounter probability (Equation(2)).

2. Detection probability as a function of depth for a lidar system with a false-alarm probability of 0.01 operating in water with an attenuation coefficient of 0.1 m^{-1}. Curves are labeled by the value of the signal-to-noise-ratio (SNR_0) at the surface.

3. Vertical distribution during daytime and nighttime used for all fishes in this paper. Data were based on anchovy. The cumulative proportion was computed from the exponential distribution.

4. Encounter probability (p_y ; Equation(1) of fish schools of 30 m diameter(Figure 4a) and 150 m (Figure 4b) for number of schools ranging from 10 to 5000, and swath width (y) from 1 m to 1600 m (y = 1, 10, 50, 100, 200, 500, 900, and 1600 m). The coastline length (L) is 133 km

5. Simulated encounter probability of anchovy fish schools in Los Angeles Bight (Table 2) for 16000, 32000 and 80000 schools, with small diameter of school group and low density of schools/ school group (multipliers of 0.5,0.5) and with multiplier (1,1). The swath width ranged from 1 m to 1600 m. Multiplier for mean and standard deviation of log (diameter of school group) and log (school density in a school group) are in parentheses. Values for populations with multiplier (1.5,1.5), close to populations with multiplier (1.0,1.0), were not shown.

6. Detection probability as a function of the false-alarm probability for lidar systems with signal-to-noise-ratios (SNR) of 1 and 3.

7. Maximum detection depth as a function of the false-alarm probability for a lidar system operating in water with an attenuation coefficient of 0.1 m^{-1}. Curves are labeled by the value of the signal-to-noise-ratio (SNR_0) at the surface.

8. Probability of detection by depth (Equation(22)) for (a) 10 cm anchovy during day- and nighttime, (b) 13 cm sardine at day and night and (c)for 20 cm and 34 cm herring during the daytime only. The vertical distributions from figure 3 are also shown for easy reference. The attenuation coefficient is 0.1.

9. Proportion of fish schools detected in the upper meter depth (Equation (23)) for 10 cm anchovy, 13 cm sardine during daytime and nighttime and for 20 cm and 34 cm herring during the daytime only. The attenuation coefficient is 0.1.

10. Proportion of fish schools detected for various SNR values at the sea surface computed for 10 cm anchovy and 13 cm sardine during day and night, 20 and 34 cm herrings during the daytime, and attenuation coefficients (α)=.05, 0.1,0.2, 0.4, and 0.6. The mean depth of anchovy during the night is 12 m, and 39 m during the daytime.

11. Depth penetration (m) for different laser energy level (J) on logarithmic scale for open ocean water and coastal water.

12. A composite image of a school derived from multiple pulses over a range of gates (depths) over time (in seconds).

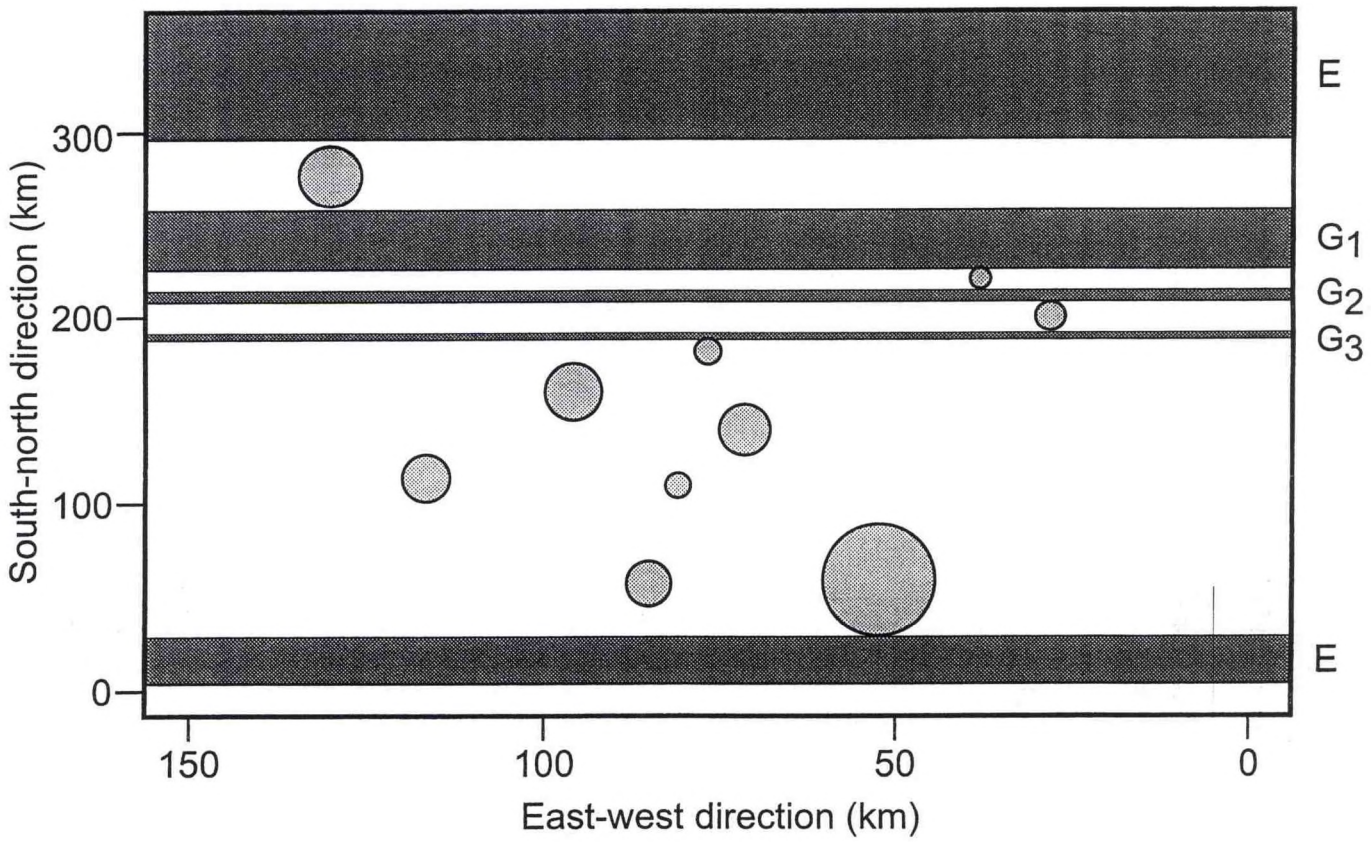
E
G1
G2
G3
E
300
200
100
0
South-north direction (km)
150
100
50
0
East-west direction (km)

Figure 1

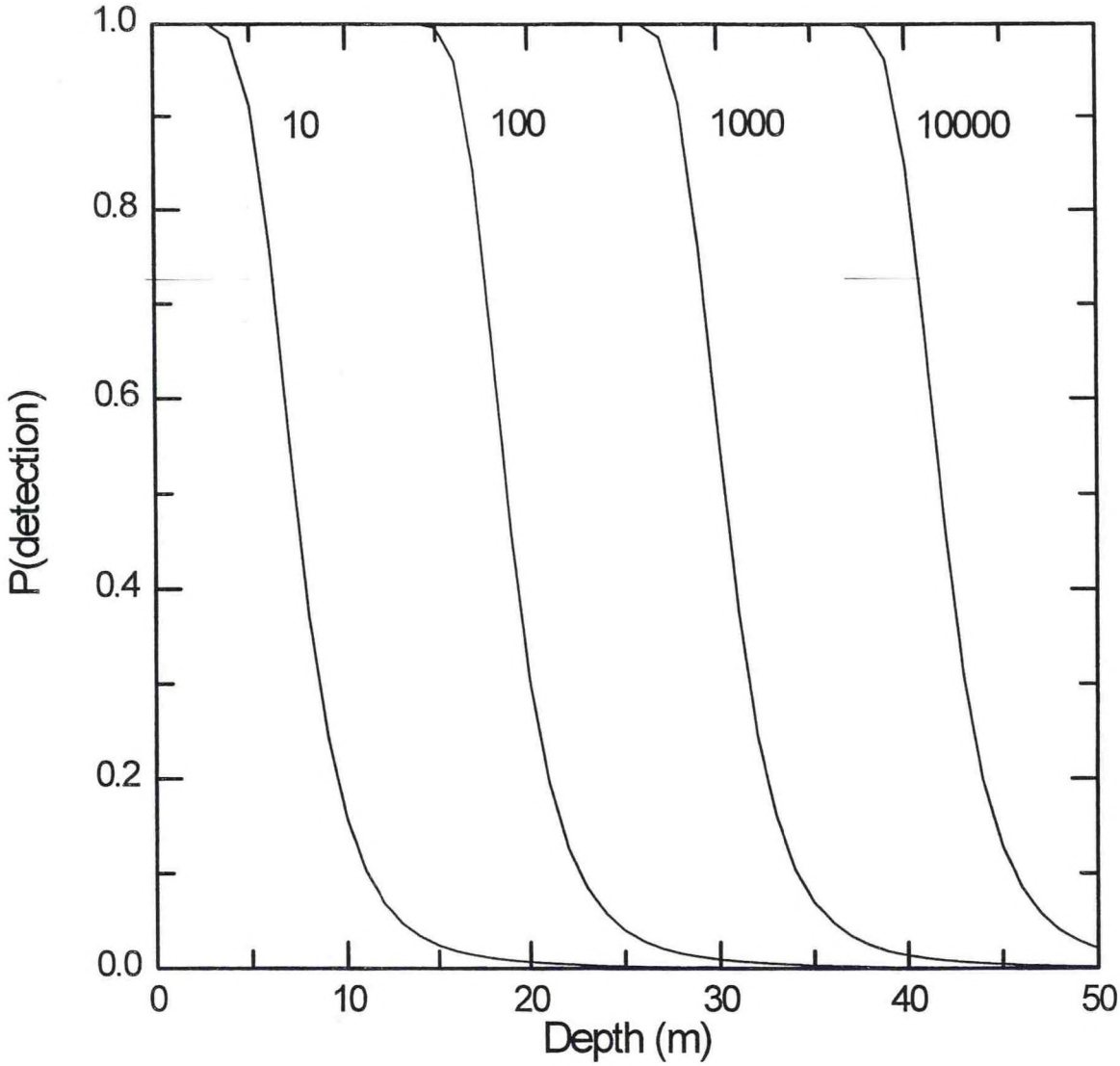
1.0
0.8
0.6
0.4
0.2
0.0
P(detection)
10
100
1000
10000
0
10
20
30
40
50
Depth (m)

Figure 2

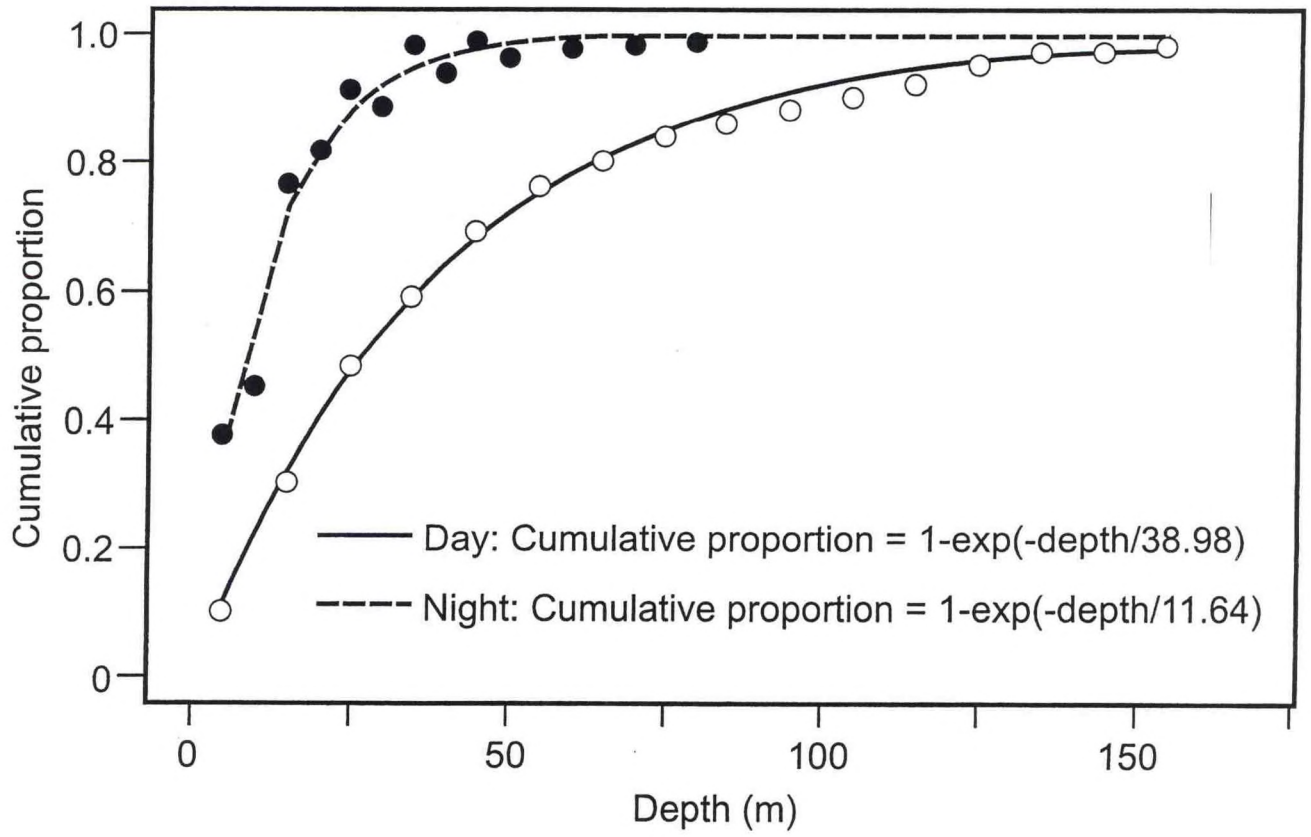
1.0
0.8
0.6
0.4
0.2
0
Cumulative proportion
0
50
100
150
Depth (m)
Day: Cumulative proportion = 1-exp(-depth/38.98)
Night: Cumulative proportion = 1-exp(-depth/11.64)

Figure 3

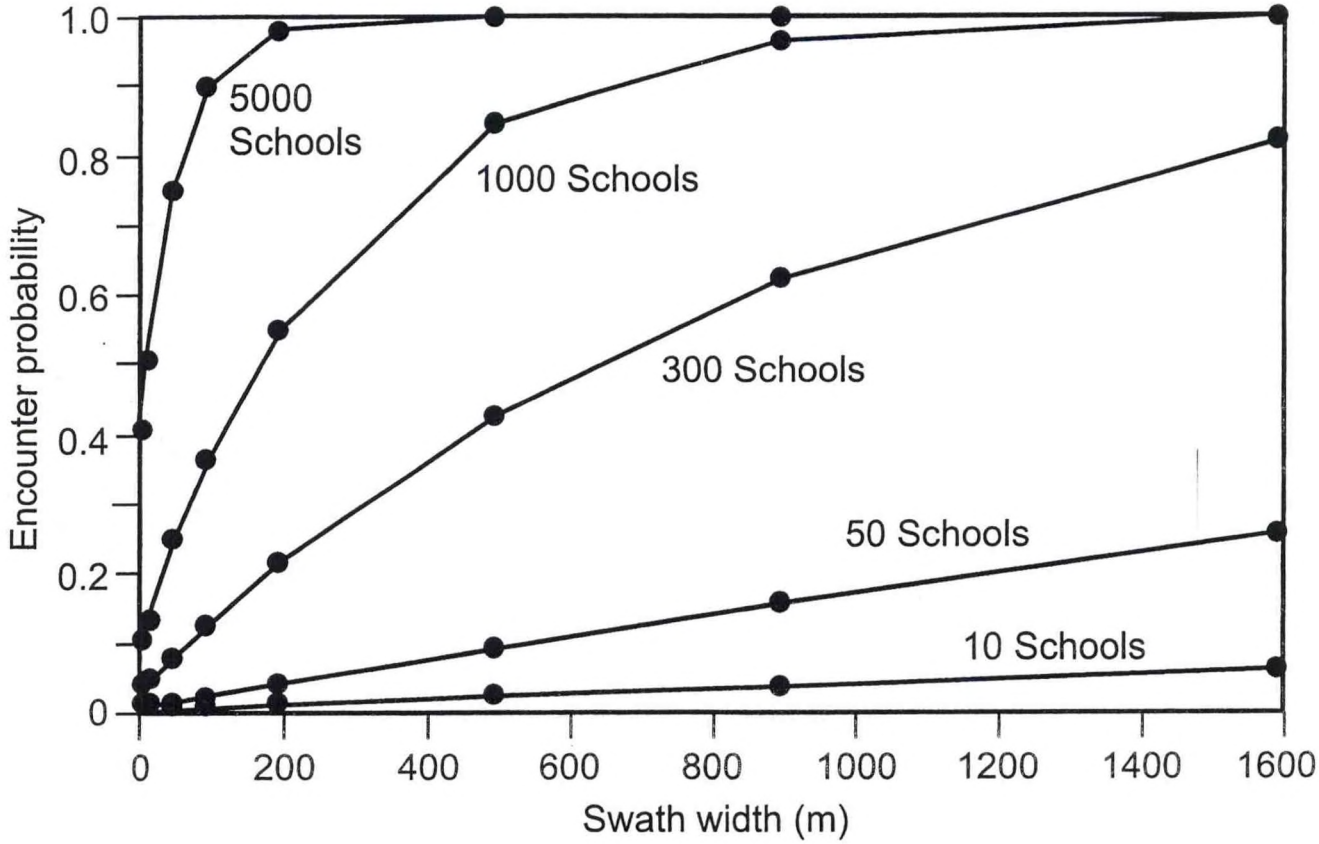
1.0
0.8
0.6
0.4
0.2
0
Encounter probability
5000
Schools
1000 Schools
300 Schools
50 Schools
10 Schools
0
200
400
600
800
1000
1200
1400
1600
Swath width (m)

Figure 4a

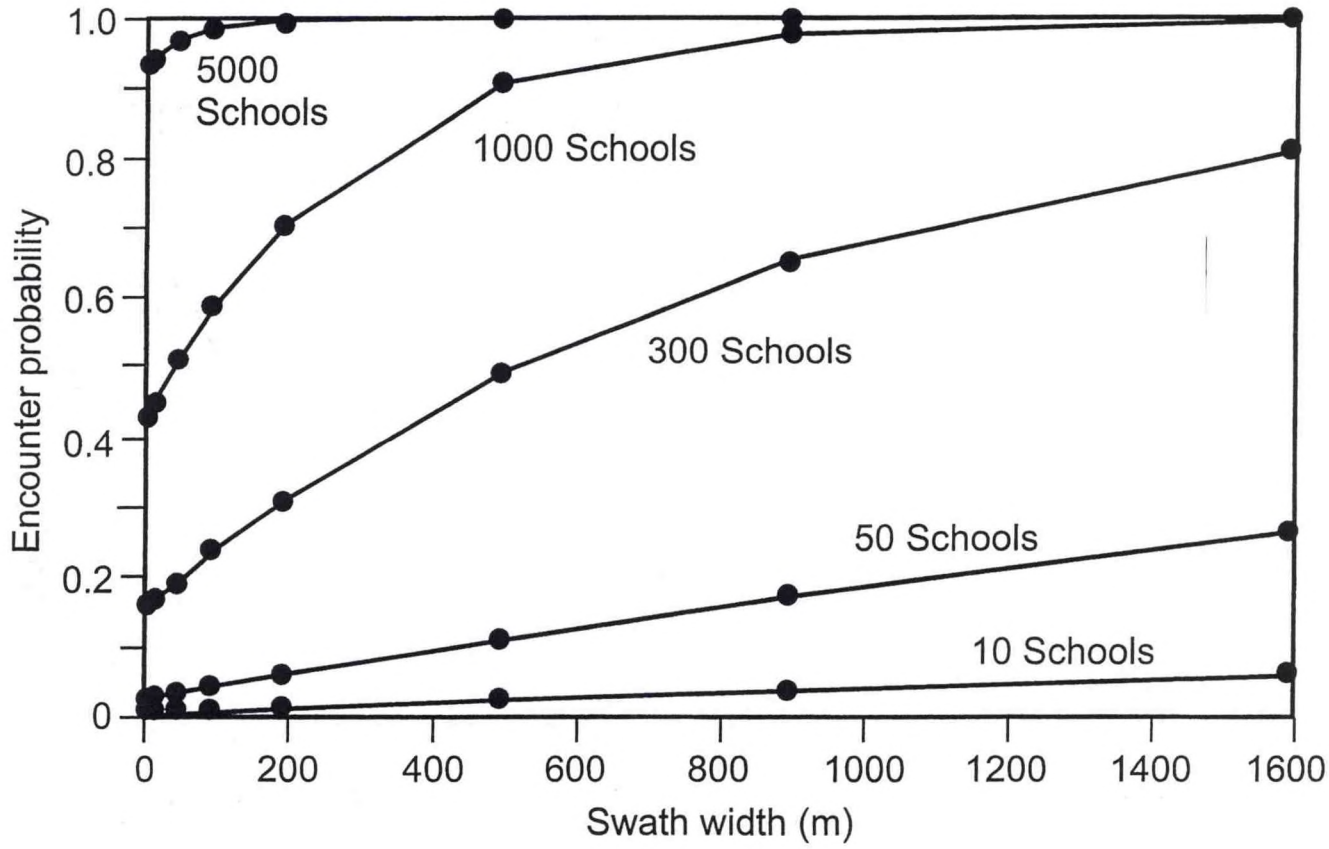
1.0
0.8
0.6
0.4
0.2
0
Encounter probability
5000
Schools
1000 Schools
300 Schools
50 Schools
10 Schools
0
200
400
600
800
1000
1200
1400
1600
Swath width (m)

Figure 4b

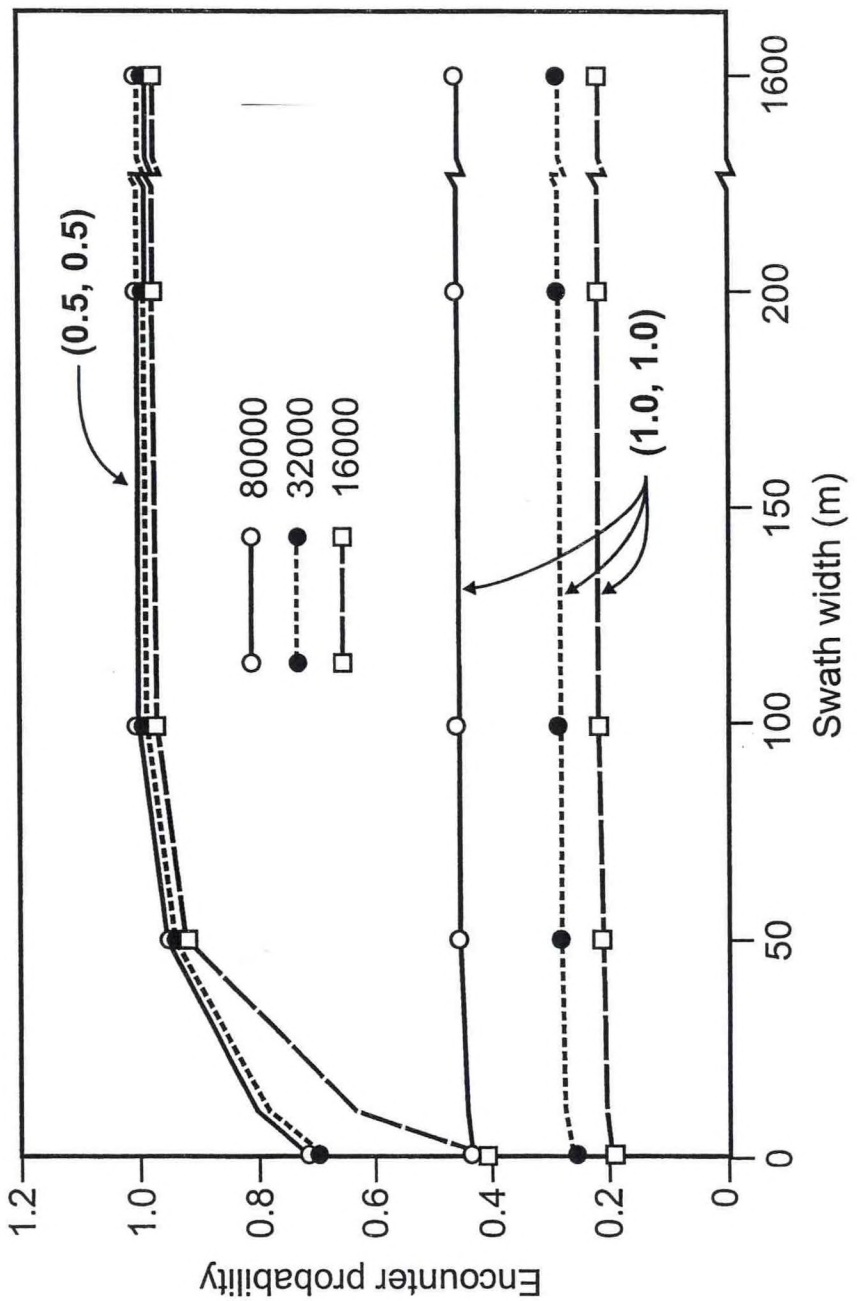
Encounter probability
1.2
1.0
0.8
0.6
0.4
0.2
0
0
50
100
150
200
1600
Swath width (m)
(0.5, 0.5)
(1.0, 1.0)
80000
32000
16000

Figure 5

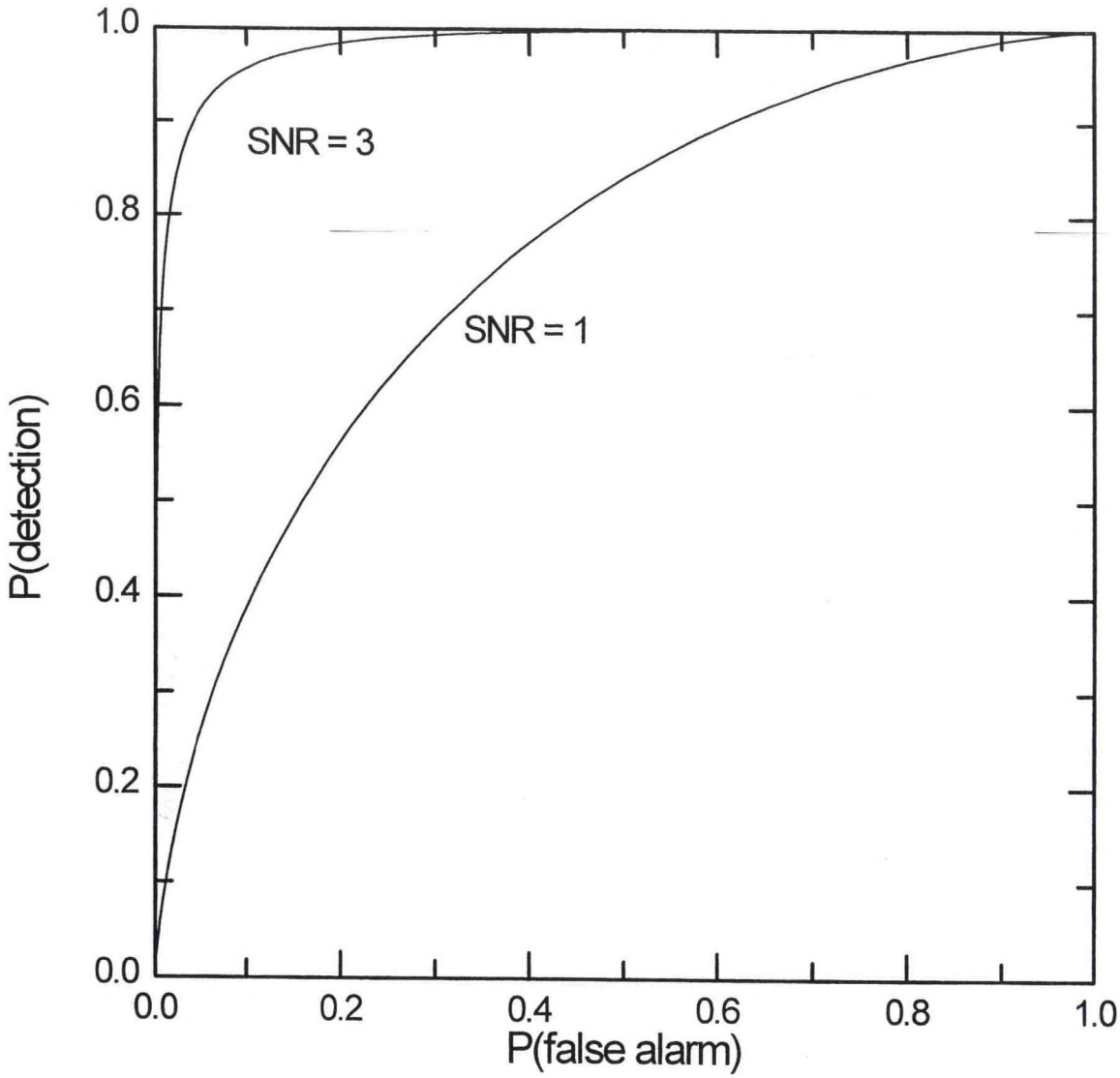
1.0
0.8
0.6
0.4
0.2
0.0
P(detection)
SNR = 3
SNR = 1
0.0
0.2
0.4
0.6
0.8
1.0
P(false alarm)

Figure 6

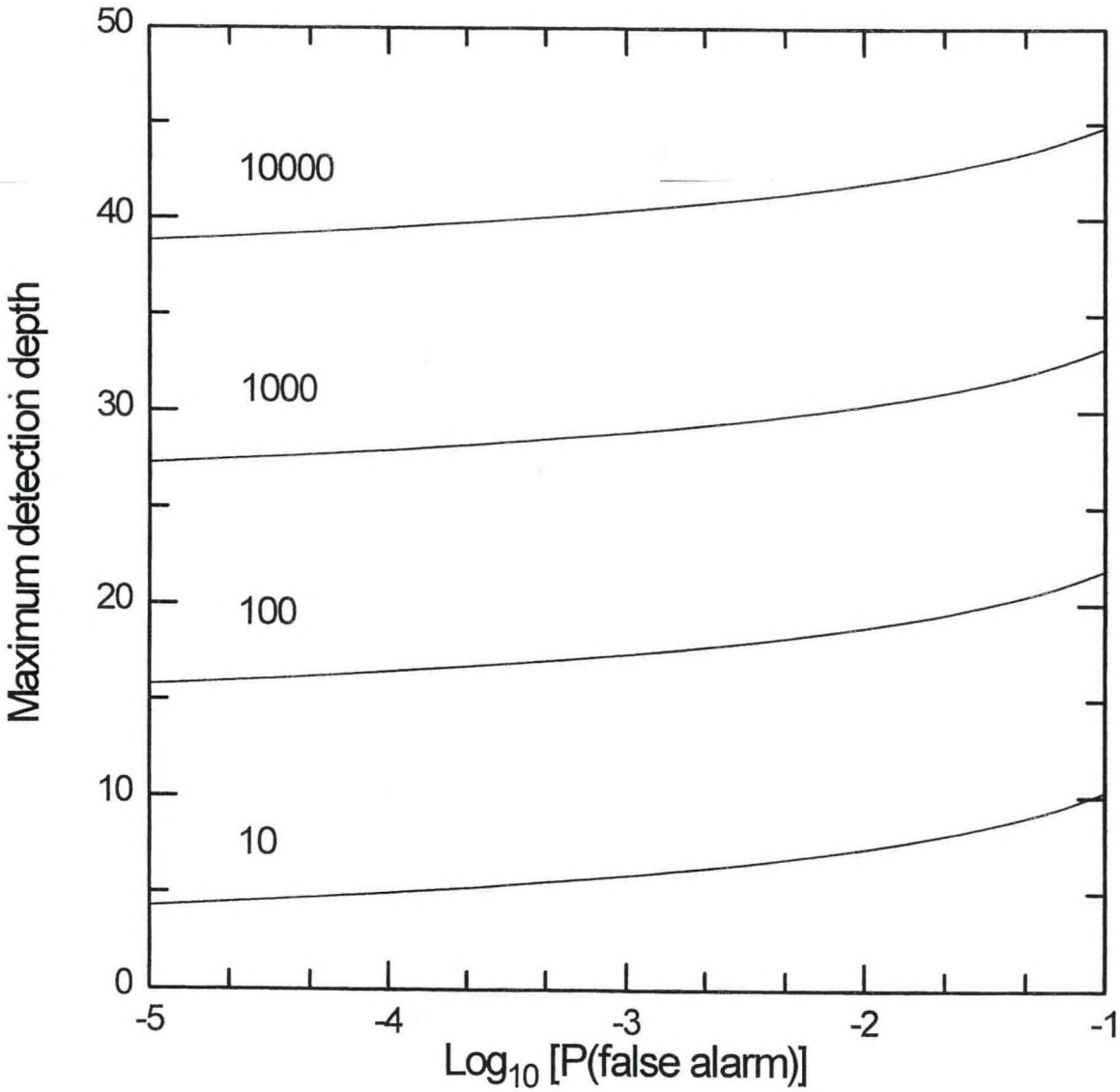
50
40
30
20
10
0
10000
1000
100
10
Maximum detection depth
-5
-4
-3
-2
-1
Log10 [P(false alarm)]

Figure 7

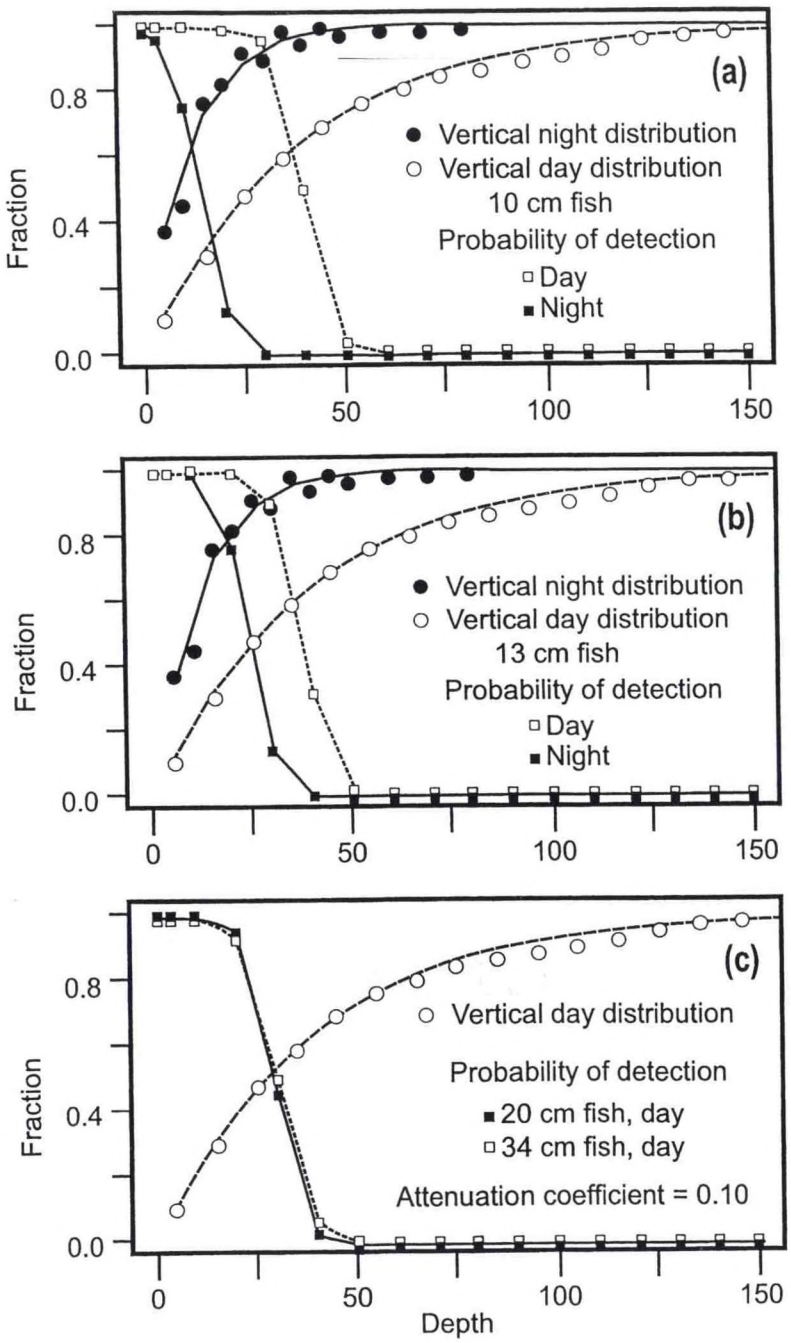
(a)
Vertical night distribution
Vertical day distribution
10 cm fish
Probability of detection
Day
Night
Fraction
0.0
0.4
0.8
0
50
100
150
(b)
Vertical night distribution
Vertical day distribution
13 cm fish
Probability of detection
Day
Night
Fraction
0.0
0.4
0.8
0
50
100
150
(c)
Vertical day distribution
Probability of detection
20 cm fish, day
34 cm fish, day
Attenuation coefficient = 0.10
Fraction
0.0
0.4
0.8
0
50
100
150
Depth

Figure 8

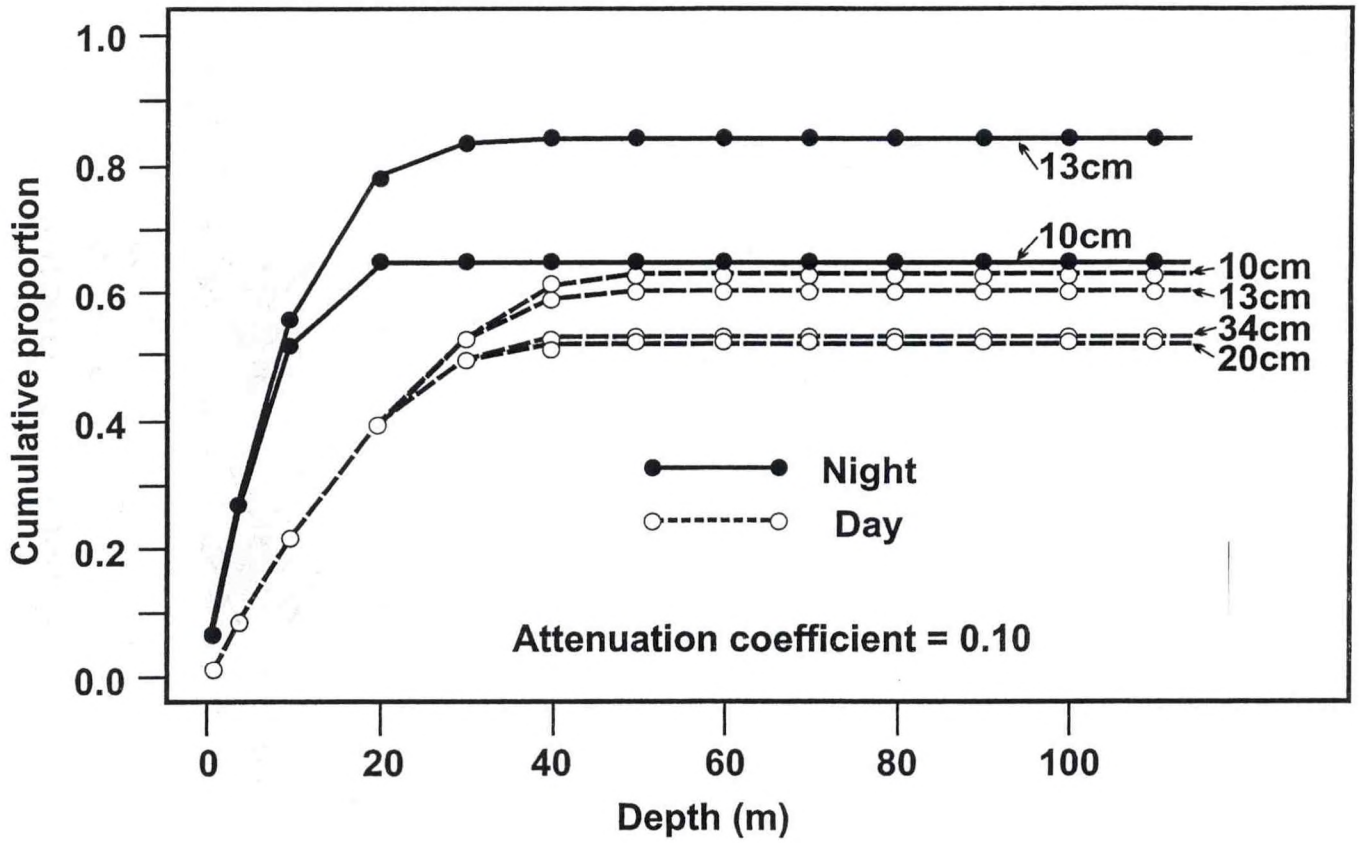
1.0
0.8
0.6
0.4
0.2
0.0
Cumulative proportion
0
20
40
60
80
100
Depth (m)
13cm
10cm
10cm
13cm
34cm
20cm
Night
Day
Attenuation coefficient = 0.10

Figure 9

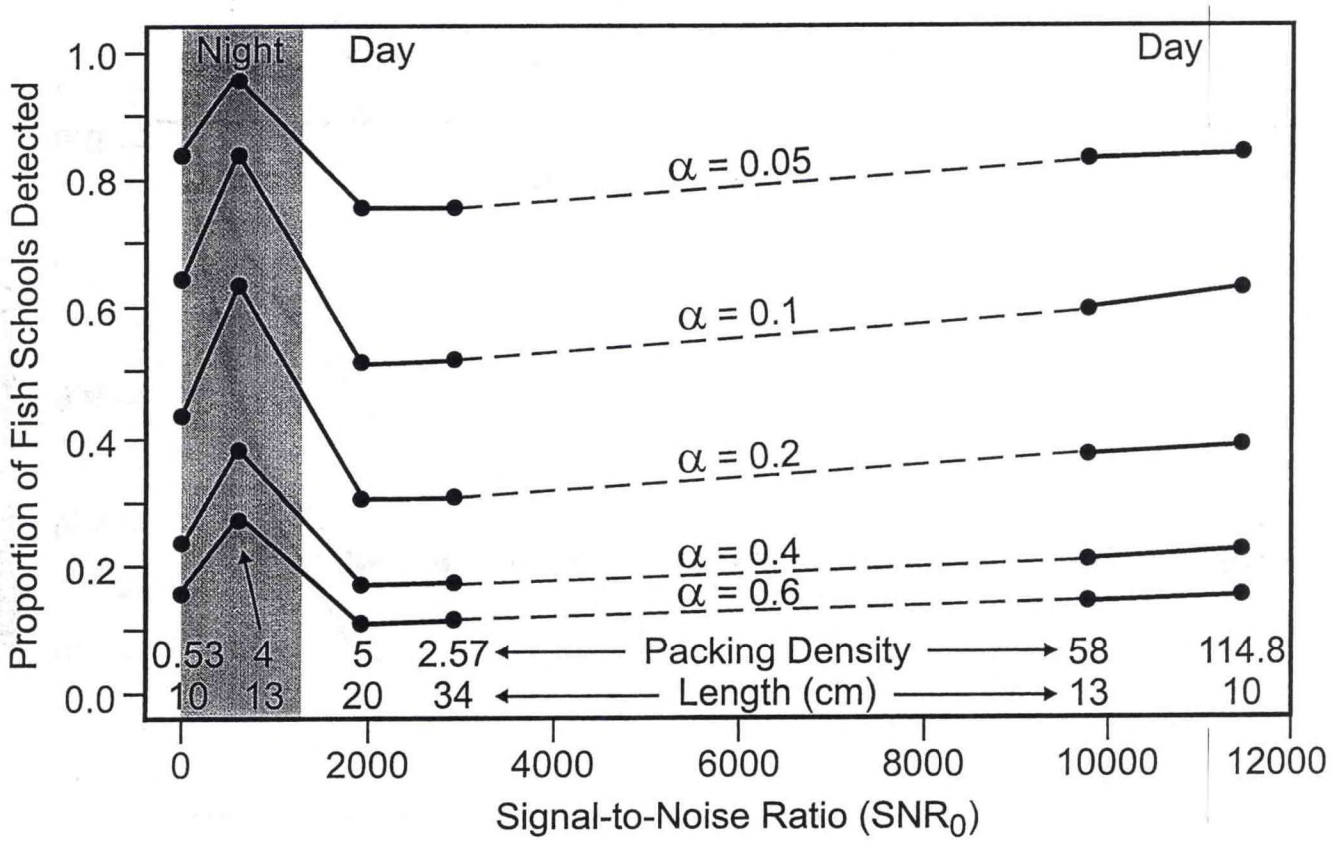
Night
Day
Day
1.0
0.8
0.6
0.4
0.2
0.0
Proportion of Fish Schools Detected
α = 0.05
α = 0.1
α = 0.2
α = 0.4
α = 0.6
0.53 4 5 2.57 ← Packing Density → 58 114.8
10 13 20 34 ← Length (cm) → 13 10
0
2000
4000
6000
8000
10000
12000
Signal-to-Noise Ratio (SNR_0)

Figure 10

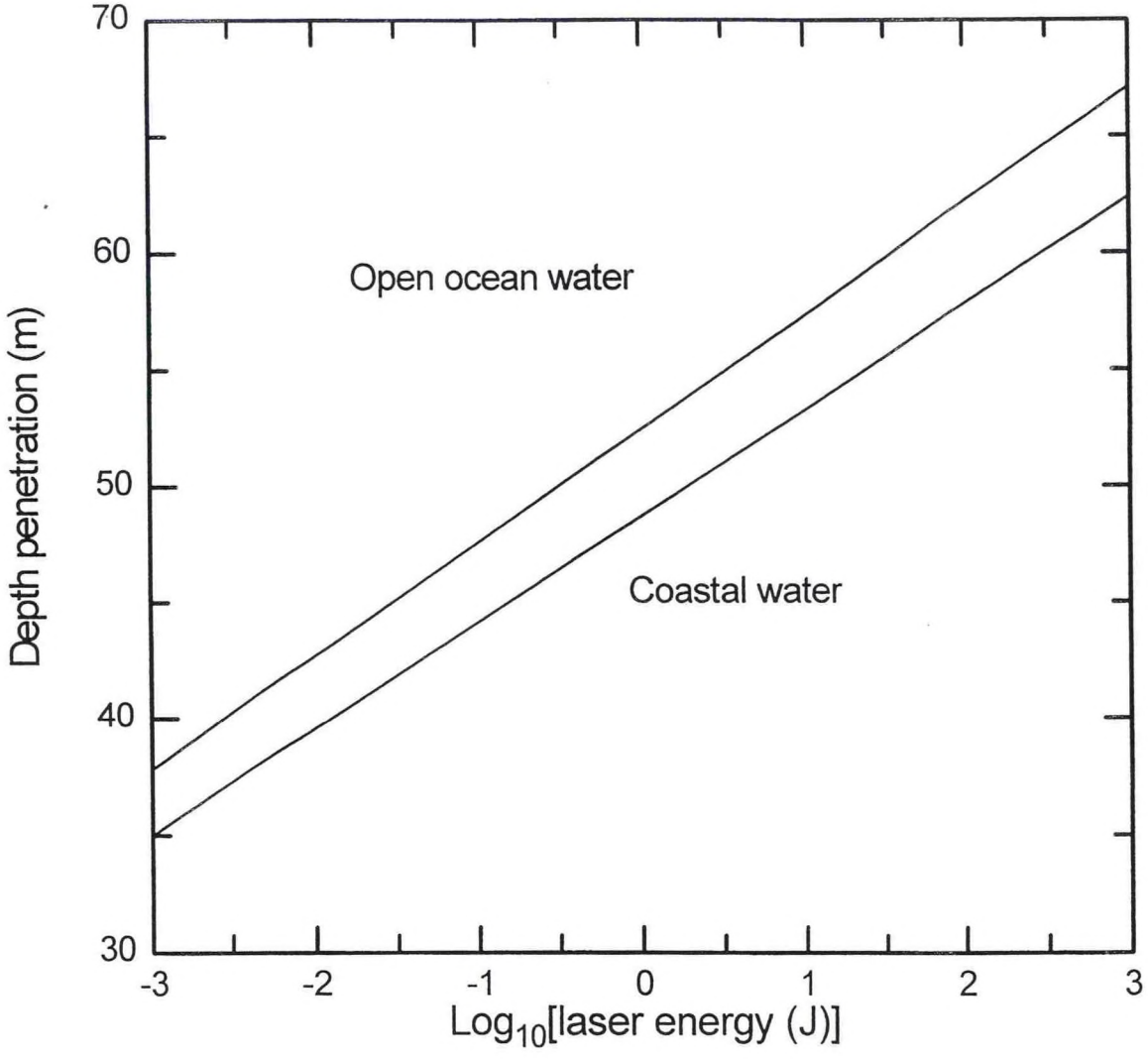
70
60
50
40
30
Depth penetration (m)
Open ocean water
Coastal water
-3
-2
-1
0
1
2
3
Log10[laser energy (J)]

Figure 11

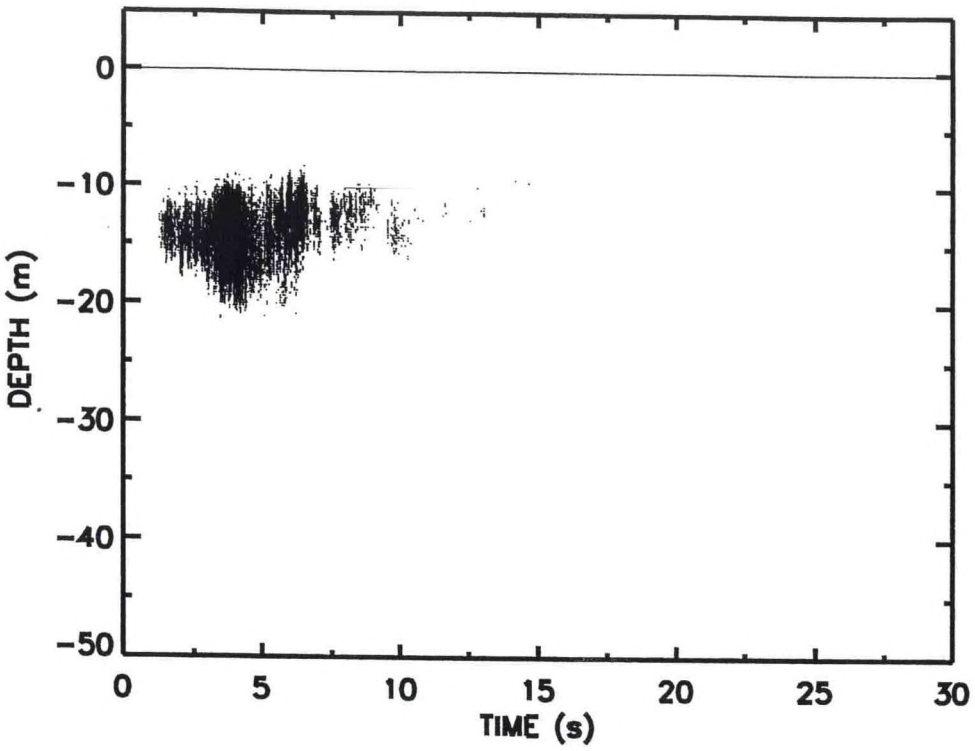

Figure 12

Table 1. The frequency distribution of school sizes of anchovy in Los Angeles Bight based on sonar mapping conducted by California Department of Fish and Game (Mais 1974; Smith 1981).

School diameter (m)	Frequency	Sample proportions
10	9906	0.4338
30	9002	0.3942
50	1822	0.0798
70	706	0.0309
90	824	0.0361
110	178	0.0078
130	217	0.0095
150	50	0.0022
170	40	0.0018
190	51	0.0022
210	19	0.0008
230	7	0.0003
250	3	0.0001
270	1	<0.0001
290	2	0.0001
310	1	<0.0001
330	3	0.0001
350	0	0
370	0	0
390	2	0.0001

Table 2. Number of school groups in one simulation run for three population levels and different diameter and density in a school group

Multiplier Diam	Density	Number of schools in a population 16000	80000	32000
0.5	0.5	221	940	365
0.5	1.0	26	122	36
0.5	1.5	8	54	23
1.0	0.5	18	9	28
1.0	1.0	5	14	7
1.0	1.5	1	13	5
1.5	0.5	2	2	1
1.5	1.0	2	3	1
1.5	1.5	1	1	2

Average number of school groups for three population sizes:

Population: 16000 schools

Multipliers for diam. of school groups	Multipliers for school density 0.5	1.0	1.5
0.5	224.79	26.28	2.71
1.0	13.32	1.56	0.16
1.5	0.56	0.07	0.01

Population: 32000 schools

	0.5	1.0	1.5
0.5	449.58	52.56	5.41
1.0	26.64	3.11	0.32
1.5	1.13	0.13	0.01

Population: 80000 schools

	0.5	1.0	1.5
0.5	1123.94	131.41	13.53
1.0	66.59	7.79	0.80
1.5	2.81	0.33	0.03

Average number of schools per school group

	0.5	1.0	1.5
0.5	71.18	608.77	5914.65
1.0	1201.33	10274.66	99826.39
1.5	28429.65	243150.98	2362398.24

Table 3. Baseline Model Parameters for computing laser power and penetration depth.

Parameter	Value
Transmitter	
Wavelength	532 nm
Pulse length	15 nsec
Pulse energy	1 mJ - 1 kJ
Pulse repetition rate	10 Hz
Height above surface	100 m
Beam divergence	25 mrad
Receiver	
Aperture diameter	20 cm
Field of view	25 mrad
Optical bandwidth	10 nm
Electronic bandwidth	100 MHZ
Sample rate	1 GHz
Receiver Noise	140 microvolts
Detector Type	R5800 Photomultiplier Tube @ 1200 V
Polarization	Un-Pol
Environment	
Aircraft Height	100 m
Water Type	IB, III
Background light	1/4 moon
Background Light Fluctuations	2 percent
Fish School	
Fish Type	Sardine
Length	13 cm
Reflectivity	
Packing Density	4 m^{-3}
School Thickness	10 m

Table 4. Estimated mean, standard deviation (SD) of packing density(n/m^3) ,coefficient of variation (CV= SD/mean) of fish of various length (10 -34 cm) during day and night and the log transformed data. The estimated school diameter were also given.

Species	Night/ Day	School Diameter	Packing density (x) mean	SD	CV	y=ln(x) [1]Mean	[2]SD	Fish length	References
Anchovy	night	30 m	0.53	0.257	0.48	-0.74	(0.52) 1.11	10 cm	Aoki and Inagaki 1988
Anchovy	day	30 m	114.8	99	0.86	4.505	(0.67) 1.11	10 cm	Grave 1977
Sardine	night	20-200m	4	----	----	0.78	1.11	13 cm	Freon et al. 1996
Sardine	day	20-200m	58	----	----	3.44	1.11	13 cm	Freon et al. 1996
Herring	day		5	-----	---	1.00	1.11	20 cm	Misund 1993
Herring	day		2.57	3.99	1.55	0.0725	1.344	34 cm	Misund 1993

[1]mean of y(= log(x)) without observed SD was computed as $\ln(\bar{x}) - 1.11^2/2$ (equation 21)

[2]SD=1.11 =sqrt(ln (1.55^2+1)) where 1.55 is the CV for 34 cm herring (equation(20)). Values in parentheses were computed from original data sets.

Table 5. The probability that at least one swath intercepts with any fish school for school diamters of 30 m and 150 m ($p_{y,n}$; equation (3)), various swath width <1 m to 1600 m and a total of 300 schools and 1000 schools when number of swaths varied from 5 to 25.

	Number of swaths (n)				
	5	10	15	20	25
School diameter = 30 m					
for 300 schools					
Swath width (m)					
<1	0.137	0.255	0.357	0.446	0.522
10	0.183	0.333	0.456	0.556	0.637
50	0.349	0.577	0.725	0.821	0.883
100	0.478	0.728	0.858	0.926	0.961
200	0.702	0.911	0.973	0.992	0.997
500	0.938	0.996	0.999	0.999	0.999
900	0.994	0.999	1	1	1
1600	0.999	1	1	1	1
for 1000 schools					
Swath Width (m)					
<1	0.415	0.658	0.800	0.883	0.931
10	0.496	0.746	0.872	0.935	0.967
50	0.761	0.942	0.986	0.996	0.999
100	0.896	0.989	0.998	0.999	0.999
200	0.981	0.999	0.999	1	1
500	0.999	1	1	1	1
>900	1	1	1	1	1
School diameter = 150 m					
for 300 schools					
Swath width (meter)					
<1	0.533	0.782	0.898	0.952	0.977
10	0.556	0.803	0.912	0.961	0.982
50	0.644	0.873	0.955	0.984	0.994
100	0.729	0.926	0.980	0.99	0.998
200	0.838	0.973	0.995	0.999	0.999
500	0.965	0.998	0.999	0.999	1
900	0.995	0.999	1	1	1
1600	0.999	1	1	1	1
for 1000 schools					
<1	0.926	0.994	0.999	0.999	0.999
10	0.939	0.996	0.999	0.999	0.999
50	0.970	0.999	0.999	0.999	1
100	0.987	0.999	0.999	1	1
200	0.997	0.999	1	1	1
500	0.999	1	1	1	1
<900	1	1	1	1	1

Table 6. Comparison of the effectiveness of laser and aerial observation with different swath width (y) and depth-penetration (z) for fish of length 10 - 34 cm during the night (n) and day (d). p_y is the probability of encountering schools for a population of 32,000 schools and swath width y. q is proportion of fish school detected for α = 0.1 and 0.05 where α is the instantaneous attenuation rate. The product, P_yq, is used to evaluate the efficiency of instruments.

α =0.1

	maximum detection depth (z) (m)	swath width (y) (m)	p_y	Proportion of fish schools detected (q)					
				10 cm Anchovy		13 cm Sardine		20 cm 34 cm Herring	
night/day				n	d	n	d	d	d
LIDAR		7	0.42	0.65	0.63	0.85	0.60	0.52	0.53
AERIAL	4	1600	0.51	0.28	0.095	0.28	0.095	0.095	0.095

	Over all efficiency (p_yq)					
	10 cm Anchovy		13 cm Sardine		20 cm 34 cm herring	
night/day	n	d	n	d	d	d
LIDAR	0.27	0.26	0.35	0.25	0.22	0.22
AERIAL	0.14	0.048	0.14	0.048	0.048	0.048
Ratio	1.92	5.41	2.45	5.21	4.58	4.58

α=0.05

	maximum detection depth (z) (m)	swath width (y) (m)	p_y	Proportion of fish schools detected (q)					
				10 cm anchovy		13 cm sardine		20 cm	34 cm
								Herring	
night/day				n	d	n	d	d	d
LIDAR	7		0.42	0.84	0.85	0.96	0.83	0.76	0.77
AERIAL	4	1600	0.51	0.280	0.095	0.280	0.095	0.095	0.095

	Over all efficiency ($p_y q$)					
	10 cm anchovy		13 cm sardine		20 cm Herring	34cm
night/day	n	d	n	d	d	d
LIDAR	0.35	0.35	0.40	0.35	0.32	0.32
AERIAL	0.140	0.048	0.140	0.048	0.048	0.048
Ratio	2.44	7.50	2.85	7.61	6.67	6.67